Hydrodynamic Interactions and Collective Dynamics of Multiple Inclusions in Two-Dimensional Membranes

by

Kaitlyn A. Parsons

A thesis submitted to the faculty of the

University of Colorado in partial fulfillment

of the requirements for the degree of

Bachelor of Science

Department of Physics

Defended March 31, 2016

Thesis Advisor:

Joseph MacLennan, Department of Physics

Defense Committee:

Joseph MacLennan, Department of Physics

John Cumalat, Department of Physics

Adam Norris, Department of Applied Mathematics

This thesis entitled:
Hydrodynamic Interactions and Collective Dynamics of Multiple Inclusions in Two-Dimensional Membranes
written by Kaitlyn A. Parsons
has been approved for the Department of Physics

Joseph MacLennan, Department of Physics

John Cumalat, Department of Physics

Adam Norris, Department of Applied Mathematics

Date

The final copy of this thesis has been examined by the signatories, and we find that both the content and the form meet acceptable presentation standards of scholarly work in the above mentioned discipline.

Parsons, Kaitlyn A. (B.S., Engineering Physics and Applied Mathematics)

Hydrodynamic Interactions and Collective Dynamics of Multiple Inclusions in Two-Dimensional Membranes

Thesis directed by Joseph MacLennan, Department of Physics

The hydrodynamics of multiple inclusions in two-dimensional, thin films of smectic liquid crystal material are studied. The self-mobilities of these inclusions are experimentally studied in highly crowded conditions by analyzing their Brownian motion. Saffman and Delbruck found the characteristic length, known as the Saffman length, beyond which momentum in a two-dimensional film has a negligible effect on an inclusion which is proportional to the thickness of the film. The effects of crowding are studied by varying the number of the nearest neighboring inclusions within one Saffman length. The self-mobilities of these inclusions are also experimentally studied for two islands of identical radii interacting within a couple of Saffman lengths experiencing an external force. This is achieved by the method of images. The interaction of two islands moving towards each other and along side each other is achieved by tilting the two-dimensional film. These two cases are thus experimentally studied by measuring the self-mobilities for islands moving perpendicular to the boundary and parallel to the boundary.

Dedication

I dedicate this thesis to my Mum, my Dad and my sister Elizabeth for all of their unwavering love and support.

Acknowledgements

Dr. Joe MacLennan, Dr. Cheol Park, Dr. Zhiyuan Qi, John Papaioannou, Kyle Meienberg, Adam Green, Dr. Zoom Nguyen, Dr. Tatiana Kuriabova, Dr. Matt Glaser, and Dr. Noel Clark.

Contents

Tables

Table

Figures

Figure

Chapter 1

Introduction

Diffusion of particles in thin two-dimensional films is the fundamental mechanism for nutrient transport in biological cells and membranes. Available literature pertaining to diffusion of objects in three-dimensions is extensive, yet there is relatively very little information regarding diffusion in two-dimensions. The observation of free-standing films of liquid crystals in the 1970's initiated many theoretical and experimental studies of suspended inclusions[1, 2, 3, 4]. Diffusion of isolated inclusions is similarly providing the frame work for the study of many-inclusion systems. Two different systems of inclusions are explored in this thesis. The first is the many-inclusion system, the second is of mutually interacting inclusions experiencing an external force. Before experimental details are discussed, motivation from scientific literature is provided. The rest of this chapter is dedicated to outlining the background information and theory necessary for these two experiments.

1.1 Purpose of Study

Scientific inquiry regarding the motion of inclusions in thin membranes is of great interest because of its applicability to understanding the physics governing multifunctional organisms in the low Reynolds number regime of fluid dynamics. Diffusion of macromolecules is the main mechanism for the transport of nutrients throughout cells. Proteins diffusing in cell cytoplasms are of interest because the molecular crowding within the cytoplasm provides a complex framework that is currently not well understood due to the numerous interactions of the crowded inclusions [5]. Furthermore, protein diffusion in crowded systems limits or drives different systems of reactions and transportation of macromolecules [6]. Neurobiology relies extensively on the study of diffusion of particles in crowded environments. Receptor targets and neuron transmitters depend on diffusion to maintain functioning of the brain [7]. Due to the complexity of studying hydrodynamic interactions of many inclusion systems, however, the amount of literature on this topic is limited. The goal of this thesis is to study the hydrodynamic interactions of inclusions in crowded systems as well as the interactions between inclusions of equivalent size both experiencing an applied external force in order to contribute to the scientific body of knowledge looking to understand the basic cellular processes that govern life.

1.2 Liquid Crystals

Phases of matter refer to the physical states in which matter can exist. The most common three phases are solids, liquids, and gases. A change in temperature is the most widely understood mechanism for matter to change phases. Changing temperature can either increase or decrease the average energy of all of the atoms by breaking or solidifying bonds between the atoms in a material. Increasing the average energy from lowest energy to highest corresponds with the phase changes from solid, then to liquid, until the material evaporates to a gas. The critical temperatures for different matter to change phases is dependent on the atomic and molecular structure of the atoms. Plasma is often referred to as the fourth phase of matter in that it has "one definition" similar to solids, liquids and gases. Solids are defined by their repeated crystalline structure of atoms. Liquids are isotropic and have a defined volume but not a defined shape. Molecules and atoms move freely in the gas phase. Plasma has more energy than the gaseous phase to the point that the molecules begin to ionize and break apart.

Less commonly known phases that have been more recently discovered or studied than the four phases mentioned above include amorphous solids, liquid crystals and many more "modern" phases such as superconductivity and Bose-Einstein condensate. Amorphous solids and liquid crystals are both intermediate the solid and liquid phases, the former existing with higher average energy than solids and the latter existing with less average energy than liquids. Unlike solids, liquids, gases, and plasmas, liquid crystals exist in a variety of degrees of order. Liquid crystals are comprised of rod-shaped molecules and these degrees of order are characterized by the average bulk orientational and positional order of these rod-shaped molecules [4]. In 1922, George Friedel published *Mesomorphic States of Matter* in which he characterized liquid crystals into three phases: nematic, cholesteric, and smectic [8]. At high temperatures, rod-shaped liquid crystal molecules exhibit isotropic behavior like a liquid in which the molecules are fluid, with no order. At low temperatures, the molecules settle into the crystalline structure characteristic of solids. In between these phases exist a variety of liquid crystal phases. Appropriate conditions for liquid crystals enable the material to exist in some or all of the characteristic phases. Figure 1.1 illustrates the progression of order of the liquid crystal molecules as temperature increases from the crystalline phase on the far left to the isotropic liquid phase on the far right. This figure does not illustrate all of the liquid crystal phases intermediate between the crystalline solid and isotropic liquid phases, however it does illustrate the two phases, nematic and smectic A, that the molecule used in my experiment exhibits.

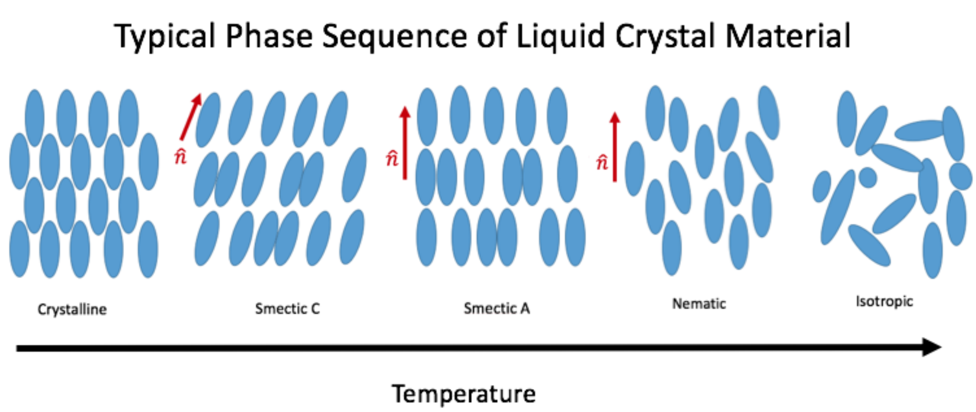

Figure 1.1: A liquid crystal material that exhibits the smectic and nematic phases will do so starting in the crystalline phase and evolve as temperature increases through the smectic and then nematic before reaching the isotropic phase.

In the nematic phase, the rod-shaped liquid crystal molecules have an average orientation pointing along a single axis known as the director $\hat{n}$ as seen in Figure 1.1 and in Figure 1.2 (c). Viscosity is lower in $\hat{n}$ than the viscosity side-to-side so the molecules move more easily in the direction of $\hat{n}$. An analogy is uncooked, rigid spaghetti noodles on a table that flow easily along $\hat{n}$, but do not tend to move in the direction perpendicular to the director. Anisotropic behavior is achieved when the alignment of the molecules if very large. Minimal alignment results in molecules most closely displaying isotropic behavior. Nematic means "thread" in Greek and was chosen for this phase of liquid crystal because the texture of the material exhibit brush-like strokes when viewed under the microscope.

In the cholesteric phase, also known as the chiral nematic phase, the rod-shaped liquid crystal molecules organize on average parallel to the director such as in the nematic phase but now display a helical structure normal to the layers. This axis about which each layer rotates, known as the chiral center, is perpendicular to the optical axis. The distance it takes the molecules to complete a period of rotation is called the pitch. Temperature and chemical composition change the pitch and this characteristic distance is very useful in order to selectively reflect light that has a wavelength proportional to the pitch. Figure 1.2 (d) illustrates the helical arrangement of the liquid crystal molecules characteristic of the cholesteric phase. The point of rotation is at the center of the rod-shaped molecule. Thus, the pitch is the distance required for the molecules to complete a 180 degree rotation.

In the smectic phase, named after the Greek word for "soap", the rod-shaped molecules organize into layers that are as thick as the length of the molecule, in addition to having orientational order. Unlike the nematic phase, translational order is present in the smectic phase, meaning the molecules flow like a fluid within each layer. There are numerous variations of the smectic phase, the two most common phases being the smectic A phase and the smectic C phase. In the smectic A phase, the molecules point perpendicularly to the layer plane, portrayed below in Figure 1.2 (a). In the smectic C phase, the molecules are arranged as in the smectic A phase but with a tilt angle measured from the perpendicular axis normal to the layer plane as shown in Figure 1.2 (b).

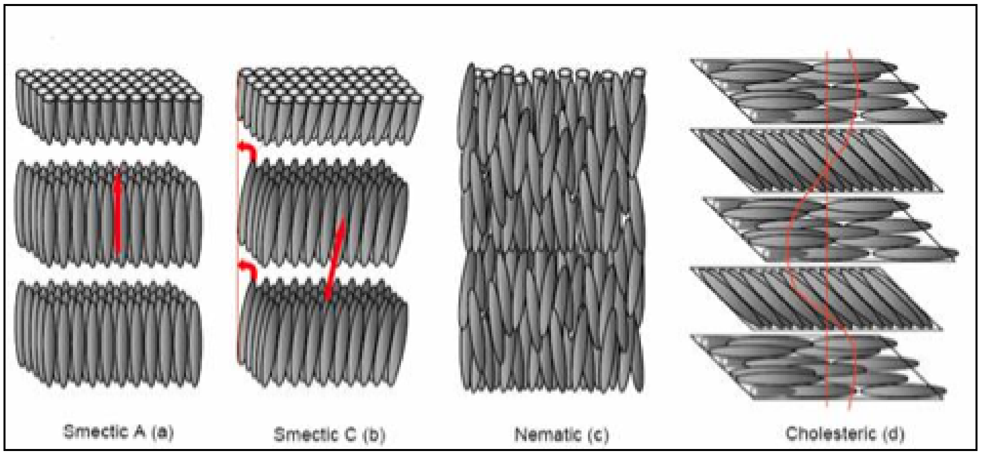

Figure 1.2: (a) The smectic A liquid crystal phase is characterized by quantization of layer by molecule length and the molecules point on average parallel to the red director axis. (b) The smectic C liquid crystal phase is characterized by layer quantization where the molecules point on average tilted away by some angle from the normal axis to each layer. (c) The nematic phase has one degree of freedom along the director axis of the molecules. (d) The cholesteric phase is a chiral nematic phase with the rotation illustrated with the red curve and the pitch the length of the straight red line [9].

Not all forms of matter exhibit the liquid crystal phase primarily due to the size and shape of the molecules and whether the molecules have a rigid and flexible part necessary for liquid crystal phases. For instance, water molecules are much smaller than a typical liquid crystal molecule and lack the rigid, rod-shape that provide directional preference based on the strength of the molecules. Thus, water molecules do not exist in the liquid crystal phase as it transitions from an ice solid to an isotropic water, or vice versa. Similarly, not all liquid crystal materials exhibit all of the possible phases due to chemical structure. Some liquid crystals only exist in the smectic A phase, others only exist in the smectic C phase, and some exhibit both of these phases. The smectic A phase typically exists at higher temperatures than the smectic C phase. However, temperature is not the only factor for when the liquid crystals transition into the various phases. Pressure also contributes as well as the density of liquid crystals in a material. In general, anisotropic molecules tend to produce liquid crystal phases but the shape and chemical composition are often insufficient information for determining the phase diagram of the material.

1.3 Material Properties of the 8CB Molecule

The liquid crystal material used throughout these experiments is 4'-n-octyl-4-cyano-biphenyl (8CB) exhibits the smectic A and the nematic phases. The abbreviation 8 denotes the number of carbon atoms in the alkyl chain which is the tail of the molecule. The abbreviations C and B denote the cyano head group and the biphenyl rings comprising the molecule's head, respectively. The biphenyl rings provide the molecular rigidity characteristic of liquid crystals. The 8CB molecule is portrayed in Figure 1.3.

8CB was discovered in the 1970's along with the discovery and widespread study of free-standing films discussed in the next section []. This molecule is very well studied in literature and many of its bulk material characteristics are well known, including the length of the material, the viscosity, and the index of refraction. The length of each 8CB molecule, and hence the thickness of each layer in the smectic A phase, is 3.17 nm [10]. The density of 8CB is $\rho \approx 0.96\ g/cm^3$ [1] with a viscosity of $\eta_{8CB} = 0.052$ Pa $\cdot$ s at temperature $T = 22°C$ [11] and an index of refraction $n_{8CB} = 1.516$ [12]. The viscosity of the surrounding still air is $\eta_{air} = 1.827 \times 10^{-5}$ Pa $\cdot$ s [13]. The values of these properties are necessary when studying the hydrodynamics of inclusions in films of 8CB.

8CB exhibits a crystalline structure at temperatures less than $20°C$ [14]. As temperature increases to the range $20° - 34°C$ the 8CB exists in the smectic A phase. The nematic phases exists for 8CB in the temperature range of $34° - 41°C$ and the isotropic phase exists for temperatures greater than $41°C$. The phases of 8CB are portrayed in Figure 1.3.

Since 8CB is in the smectic A phase at room-temperature, it is ideal for studying two-dimensional hydrodynamics within lab conditions that are easily maintained. No heating oven or cooling mechanism is required when working with this material. The smectic A phase exists over a relatively large temperature range so small fluctuations in the temperature of the lab do not affect the physical properties of the material, such as the material's viscosity. If the temperature range for the phase of interest is too small, then depositing inclusions that are interacting with each other can heat the film. This is not a concern when using 8CB. The price of 8CB has decreased with time since its discovery, making it exceptionally cheaper than some of the newer liquid crystals.

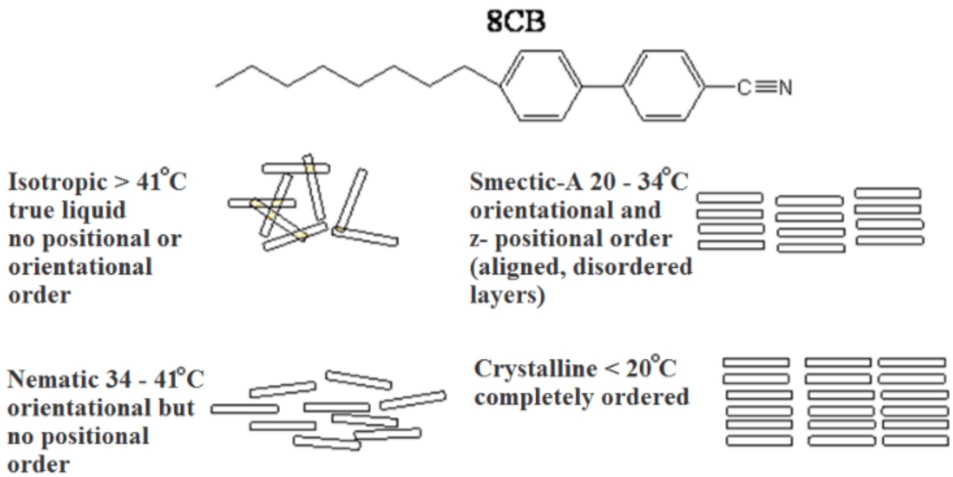

Figure 1.3: The 8CB liquid crystal molecule along with the different phases it exists with and the corresponding temperature range of each phase [14].

1.4 Thin, Free-standing Films of Smectic A Material

Free-standing liquid crystal films are unique in that they provide an ideal platform for studying two-dimensional hydrodynamics [15]. The quantization of layer thickness in the smectic A phase provides one-dimensional order and the fluid flow within each layer provides two-dimensional disorder. These free-standing films are created across a hole in a thin piece of glass referred to as the film holder. The diameter of this hole can range from a few millimeters to a couple of centimeters. A small amount of the liquid crystal material is then placed on the edge of the hole and another small piece of glass is used to spread the material over the hole. This procedure, depicted in the cartoon illustration in Figure 1.4, results in a free-standing film of liquid crystal material [16].

An analogy to the free-standing film is to consider creating a soap film over a bubble wand. Unlike the volatile soap that consists mostly of water, free-standing liquid crystal films of 8CB do not pop

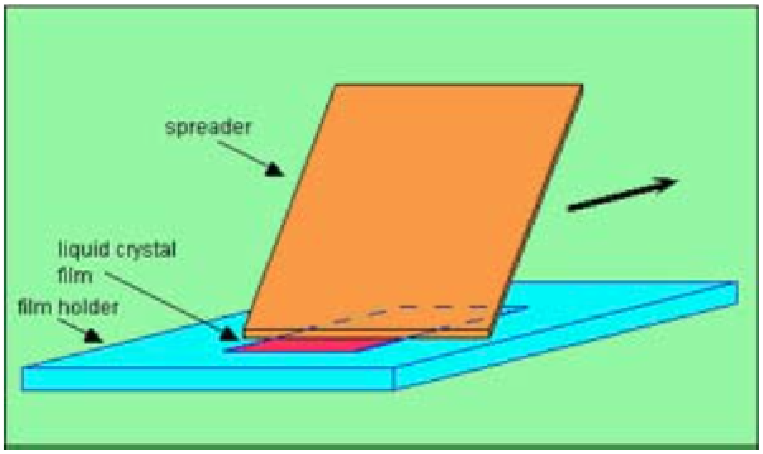

Figure 1.4: A free-standing liquid crystal film (red) is created by drawing the material with the spreader (orange) over the film holder (blue) [16].

due to evaporation because of the low vapor pressure of the liquid crystal material. Free-standing films are homogenous and stable for many hours or even for days. Tension, much like that of a drum's membrane, keeps the film flat with each layer of the film oriented parallel to the plane of the film.

Thicknesses of these films range from two to ten layers, although thinner films are more difficult to obtain, especially for larger film holder diameters. The speed at which the material is drawn over the film holder, as well as the amount of material pulled across affect the thickness of the film. Pulling the material too quickly or too slowly often results in the film popping due to the instability of the moving glass piece that acts as an edge to the creating film. Controlling the film thickness is very difficult, although pulling the material over the film holder quickly often results in thinner films. In order to obtain a film of specific thickness many films must be created as a trial and error process.

The boundary at which the film meets the film holder is surrounded by a much thicker region of material, known as the meniscus. Films that are between two to ten layers are only a few nanometers in thickness while the meniscus is up to a few hundred microns thick. This reserve of extra liquid crystal material is crucial for the creation of islands discussed in the next section.

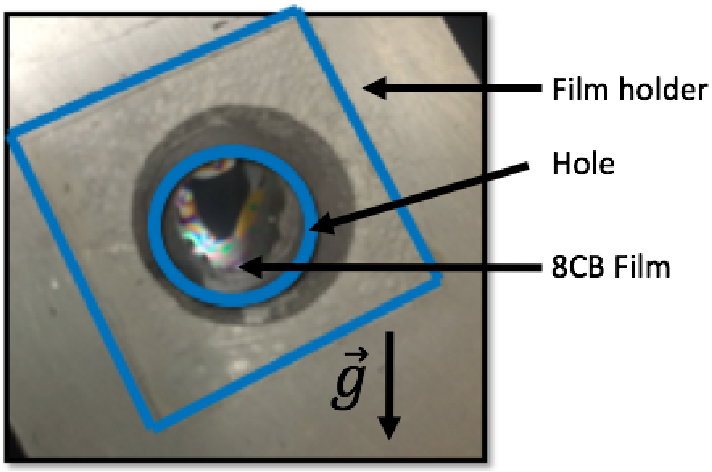

Figure 1.5: This free-standing liquid crystal film is suspended a hole in the film holder outlined by the blue circle. The glass film holder is outlined by the blue square and is mounted on an aluminum piece for easy handling. The film is held vertically with gravity indicated by $\vec{g}$.

Figure 1.5 shows one of my films of 8CB suspended in a 1 cm film holder hole outlined by the blue circle. The entire glass piece that comprises the film holder is outlined by the blue square. The film holder is mounted to a piece of aluminum with a hole drilled through for easy handling of the film under the microscope. The black region on the film within the blue circle is the thinner part of the material. The thicker region is much brighter because more light is reflected back than is transmitted through. When this picture was taken the film was held vertically, some of the 8CB material drifted under the force of gravity to the bottom of the film holder.

Two-layer films are similar to lipid bilayers that exist in biological cells. Understanding these two-layer systems is critical in understanding the physics underlying diffusion in cells. Even films of thickness greater than two layers are useful for studying these hydrodynamic influences.

1.5 Islands

The inclusions used in my experiments are called islands, which are thicker, pancake-like regions of smectic A material. They are thicker than the surrounding film and can range from a few smectic layers thick to hundreds of microns thick. The radii of these islands can also range from a few to hundreds of microns.

A water droplet is pulled into a spherical shape because this minimizes the surface area and hence minimizes the energy. Similarly, islands form cylinders because this geometry minimizes the perimeter and thus minimizes the energy. The cylindrical shape rather than the spherical shape of the water droplet is required due to the quantization of the layer thickness by the length of the 8CB molecule. The cross-section of an island suspended in a free-standing film is depicted in Figure 1.6. The meniscus is portrayed as a curved connection between the film and the film holder and is the source of the extra material used to create the islands.

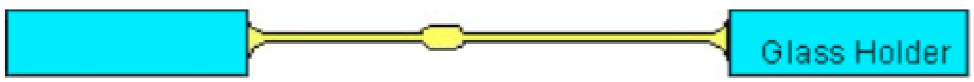

Figure 1.6: Cross-section of a free-standing film (yellow) with an island. The film is suspended in the glass film holder (blue) [17].

Molecules within the film have the ability to diffuse easily laterally to and from the meniscus, however molecules within an island diffuse much slower from layer to layer, although it is possible. When a molecule diffuses from within an island, another molecule already within the film is pushed back into the meniscus. In some smectics, islands shrink over time. The number of layers in a shrinking island remains constant as the volume of the island decreases until the island completely vanishes into the film. Thicker islands will thus have a radius decreasing at a greater rate than thinner islands. The rate at which the radius decreases can vary and must be considered when studying the hydrodynamics of the island as discussed later.

There are two models that describe how the extra layers of the islands sit relative to the film. The incorrect model is that the extra layers sit directly on top of one another and stack above and below the film depicted in Figure 2.6b. The correct model depicted in Figure 2.6a, is that the extra layers comprising the island are enclosed by the film.

(a) Correct model of island

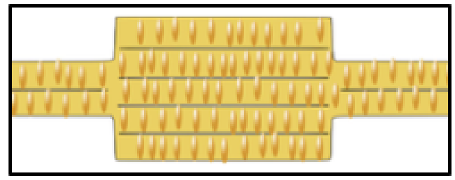

(b) Incorrect model of island

Figure 1.7: (a) Side profile of six layer film with layers enclosed by the film [17]. (b) Side profile of five layer film with layers stacked above and below film [18].

When considering a film system with many islands crowding each other, coalescence events cause considerable amount of fluid flow throughout the film. Coalescence events occur when islands interact with each other or with the meniscus and happen at a rate that is between milliseconds to microseconds or even faster. The amount of fluid flow from these events is roughly proportional to the volume of the interaction islands. Coalescence between two islands occurs when they touch edges and the smectic layers merge together allowing the material to flow.

When islands are of the same thickness, then the result is a larger island with radius greater than either of the two initial interacting islands because the strong line tension will draw each layer into a stable circular shape. In the event of an island coalescing with the meniscus, the stronger fluid pressure in the film than in the meniscus will push the entire island into the meniscus. This results in a greater meniscus region connecting the film with the film holder as seen in Figure 1.8.

The most dynamic interactions occur when islands of different thickness touch edges. The layers of the thicker island that are closest to the film will interact with the thinner island, however the layers above the thinner island are still confined to their respective layers. This results in what looks like the thinner island pulling in the thicker island. The pressure from the surrounding film can exert a large enough force that pushes the material of the thinner island into the thicker island, until the two islands reach the same radius. The final result is an island with the same thickness as the thicker initial interacting island but with a greater radius. Figure 1.8 illustrate coalescence events between two islands of different thicknesses as well as with the meniscus.

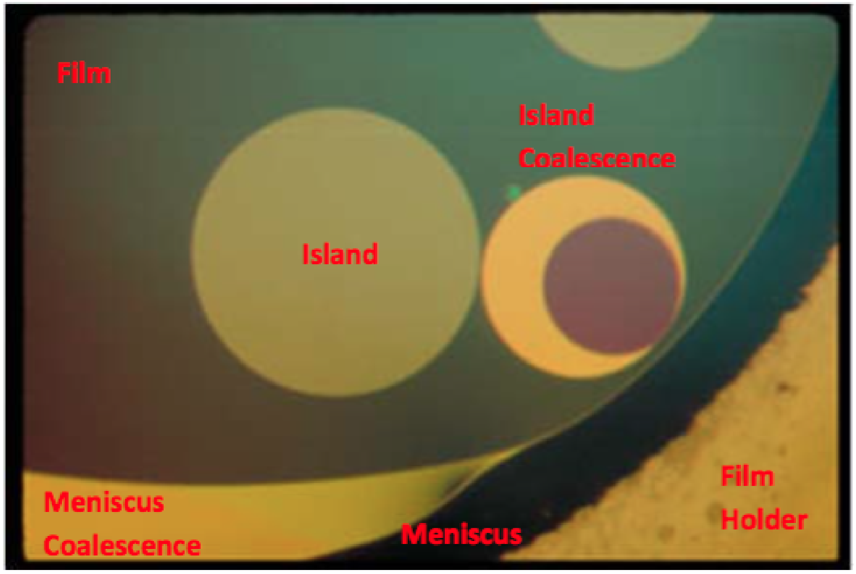

Figure 1.8: Islands that have coalesced with each other and the meniscus [16].

Interactions between islands and the meniscus, however, do not always guarantee coalescence events. Throughout these experiments it has been observed that many islands can crowd compactly without coalescing. Similarly, islands were observed to sit against the meniscus without coalescing. It is still unknown why the islands do not always coalesce such as the islands in Figure 1.9.

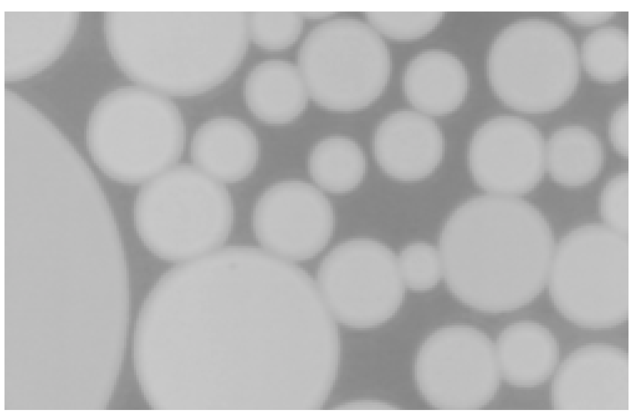

Figure 1.9: Islands that are interacting but not coalescing have squashed boundaries and thus do not look perfectly circular as they do normally.

Islands are created in these experiments through deposition of silicone oil droplets onto the film or by blowing air across the meniscus and pushing extra material onto the film. They can also spontaneously form but a high density of islands is created more effectively by means of the first two methods. My crowding experiment utilizes oil droplet deposition and air created islands while my tilted film experiment utilizes air created islands as well as spontaneously formed islands.

For oil droplet deposition I create my film and put the entire film holder in a small aluminum chamber where a wire coils around the inside of the chamber. The oil is spread lightly on the wire and the lid to the chamber is placed. Current is then sent through the wire inside the chamber evaporating the oil. Once the current is turned off, the oil condenses onto the film. After the oil droplets settle onto the film, smectic A material in the film envelopes the droplets to create stable islands. This happens because the size of the each droplet is much larger than the thickness of the film and the numerous defects in the particle's structure cause discontinuities in the layering of the smectic A material, and thus nucleate islands in order to minimize the energy.

The method of blowing air across the meniscus to create islands can create systems ranging from isolated islands to very crowded systems of islands. The experimenter can blow air across the film two main ways: with a straw and with needles attached to nitrogen. The first method is great for isolated cases and low density cases because the experimenter can view the process through the microscope and can thus gauge how much air to use based on the movement of the material in the film. Too much air results in popping of the film and not enough air does not create islands. I built a mechanism for the needle process displayed below in Figure 1.10. Two retractable needles are positioned on either side of the film and nitrogen attached to them. The positioning of the needles is crucial. If the needles are too high above the film either no islands or systems of islands that are not crowded enough are created. If the needles are too close the film will pop. The x and y coordinate positioning of the needles is also important because the number of flow regions produced by the nitrogen flow determines whether the system is highly crowded or not.

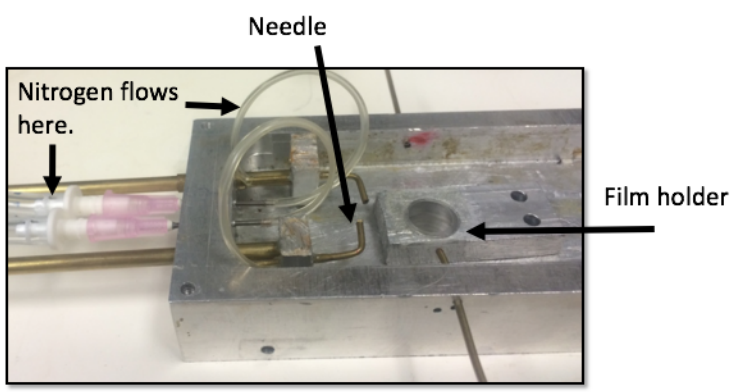

Figure 1.10: Film holder on aluminum piece is inserted into the air chamber. The nitrogen flows through the pink needles into the thin clear tubing and through the retractable gold needles.

Chapter 2

Theoretical Background

Two-dimensional hydrodynamics of an isolated particle and of two mutually-interacting particles has been studied [18]. This thesis examines two experiments that are more complex than the single particle problem. The first experiment extends interactions between two particles to a system of many particles. The second experiment studies the mutual interactions of two identical particles each experiencing an external force by using the method of reflections. This chapter provides the foundational theory necessary to study these two complex systems.

2.1 2D Hydrodynamics of Isolated Island

Brownian motion is the random movement of a particle that results from it colliding with the atoms and molecules comprising the fluid it is suspended in. In 1827, Robert Brown observed pollen amyloplasts, also known as starch organelles, randomly moving in water [19]. At the time it was believed that this random movement was characteristic only of living organisms. Brown's experiment spurred scientists to debate two avenues of thought on the fundamental nature of matter. The first avenue was that matter is comprised of fundamental particles now known as atoms. The second line of thought was that matter is comprised solely of energy. In 1905, Albert Einstein settled the debate in favor of the atomistic view. Einstein's theory suggested that the random movement of particles undergoing Brownian motion is due to the interactions between the molecules of the suspension fluid and the particle.

The two measurable quantities of Brownian motion are the diffusion coefficient and the mobility. Diffusion refers to the bulk dissipation of molecules within a fluid resulting from kinetic-molecular interactions as described by Einstein's theory. In 1822, Joseph Fourier initiated the mathematical investigation of diffusion with his publication on heat transfer [20]. The partial differential heat equation, inspired from his extended time in Egypt, is a specific application of the particle diffusion partial differential equation derived by Adolf Fick later in 1855 [21].

Translational diffusion of a particle undergoing stochastic or probabilistic movement, such as a random walk or Brownian motion, is mathematically represented by the diffusion coefficient which has units of area per time. The translational diffusion law for two-dimensions relates the mean-squared displacement, also known as the average displacement, to the diffusion coefficient as shown in Equation 2.1. The translational diffusion law was originally derived for one dimension. Since the mean-squared displacement in one direction is independent of another direction, the translational diffusion law is easily extended to two dimensions by summing the mean-squared displacements for each translation direction.

$$\langle r^2 \rangle = \langle x^2 + y^2 \rangle = 2Dt + 2Dt = 4Dt \tag{2.1}$$

Here the mean-squared displacement is $\langle r^2 \rangle = \langle x^2 + y^2 \rangle$, the diffusion coefficient is D and the lag time is t. The lag time is the amount of time the particle is given to diffuse before measuring the mean-squared displacement. Note that Equation 2.1 does not take the diffusing particle's shape and size into account.

The mobility μ is defined as the ratio of the drift velocity v_d of the particle to an applied force F as seen in Equation 2.2.

$$\mu = \frac{v_d}{F} \tag{2.2}$$

In 1851, George Gabriel Stokes determined the relationship between the mobility of a spherical object and its radius and the viscosity of the suspension fluid for the low Reynolds number regime [22]. In fluid dynamics, the Reynolds number is a dimensionless ratio of the inertial forces divided by the viscous forces a particle experiences [23]. The low Reynolds number regime refers to a particle experiencing a much greater viscous force than an inertial force. Equation 2.3 is Stokes' Law for the three-dimensional diffusion of a particle where μ is the mobility, η is the viscosity of the fluid, and a is the radius of the spherical particle.

$$\mu = \frac{1}{6\pi\eta a} \tag{2.3}$$

It wasn't until 1905 that Albert Einstein related the diffusion coefficient of a particle diffusing in any dimension with its mobility in what is known as the Einstein relation (Equation 2.4) [24].

$$D = \mu k_B T \tag{2.4}$$

Here the diffusion coefficient D is equal to the mobility μ multiplied by Boltzmann's constant k_B and temperature T. The mobility is constant in the low Reynolds number regime. Einstein's relation provides a method to experimentally determining the mobility of a particle by measuring its diffusion coefficient or determining the diffusion coefficient by calculating the mobility from the measured velocity and external applied force.

Mobility in two dimensions is less understood than in three dimensions. Stokes discovered that a disc moving through a two-dimensional film approximated as infinite at a constant velocity with zero force acting on it resulted in an infinite diffusion coefficient.

In 1975, Saffman and Delbrück (SD) proposed that the diffusion coefficient of a particle suspended in a thin two-dimensional film depends not only on the viscosity of the material of which it is suspended in but it also depends on the viscosity of the surrounding fluid, such as still air. They also determined that the diffusion coefficient falls of logarithmically as a function of the inclusion's radius and the viscosity of the surrounding fluid [3].

Saffman found that the surrounding fluid's viscosity contributes significantly to the momentum dissipation throughout the two-dimensional film, even if this surrounding fluid's viscosity is much smaller than the viscosity of the thin film material [2]. The characteristic length that determines the range until fluid flow in the film does not contribute to the motion of the island is known as the Saffman length (l_s), given by Equation 2.5 for 8CB surrounded by still air.

$$l_s = \frac{h\ \eta_{8CB}}{\eta_{air}} \tag{2.5}$$

Here h is the film's thickness, η_{8CB} is the viscosity of the liquid crystal material and η_{air} is the viscosity of the surrounding still air. The SD model, however is only appropriate for islands with radius a less than and at most equal to the Saffman length, i.e., $a \leq l_s$. The result of the calculation for the mobility in this radial regime is given in Equation 2.6 where $\gamma = .577215$ is Euler's constant.

$$\mu = \frac{1}{4\ \pi\ h\ \eta_{8CB}} \Big(ln\Big(\frac{l_s}{a} - \gamma\Big)\Big) \tag{2.6}$$

Saffman and Delbrück remarkably concluded that the mobility of the particle is independent of the thickness of the island and only dependent on the thickness of the film and the particle's radius. Two smectic islands of the same radius but of immensely different thickness thus have the same mobility. This result demonstrates that the distance by which the island protrudes out of the film and the extent to which it interacts with the surrounding fluid does not affect the mobility. This result holds for the diffusion coefficient as well since it is proportional to the mobility by the constant factor $k_B T$.

The extension of the SD model by Hughes, Pailthrope and White (HPW) analytically determined the mobility of islands for radius much greater than the Saffman length, $a \gg l_s$ [25]. Petrov and Schwille (PS) connected the SD model with the HPW model with the following expression for mobility in Equation 2.7 [26].

$$\mu = \frac{1}{4\ \pi\ h\ \eta_{8CB}} \Big(\frac{ln(\frac{2}{\epsilon}) - \gamma + \frac{4\epsilon}{\pi} - \frac{\epsilon^2}{2} ln(\frac{2}{\epsilon})}{1 - \frac{\epsilon^3}{\pi} ln(\frac{2}{\epsilon}) + \frac{c_1 \epsilon^{b_1}}{1 + c_2 \epsilon^{b_2}}} \Big) \tag{2.7}$$

In this equation, h is the film thickness, η_{8CB} is the viscosity of the film, $\epsilon = a/l_s$ is the reduced radius and the following are constants: $c_1 = 0.73761$, $b_1 = 2.74819$, $c_2 = 0.52119$, $b_2 = 0.61465$. The SD-HPW-PS model for mobility was experimentally confirmed in our lab in 2010 for isolated islands [27]. The following plot in Figure 2.1 is of the reduced mobility $m = \mu(4\pi\ \eta_{8CB}\ h)$ which is dimensionless versus the reduced radius a/l_s, also dimensionless, for films of different numbers of layers N. The inset is a graph of the diffusion coefficient versus the radius for islands in a three layer $N = 3$ film. Several sets of each radius were measured to obtain error bars corresponding to the standard deviation in the mobility.

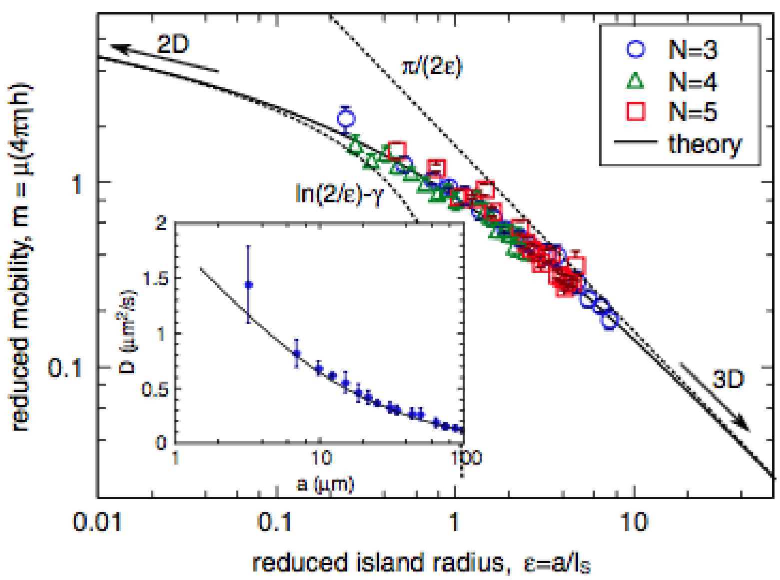

Figure 2.1: The SD model falls off logarithmically as $ln\frac{2}{\epsilon} - \gamma$ and is only valid for $a \ll l_s$. The three-dimensional behavior model continues unboundedly as $\frac{\pi}{2\varepsilon}$ as the radius approaches zero. The crossover region for the SD-HPW-PS model was experimentally verified in our lab. N is the number of layers in the film. The inset is the diffusion coefficient D versus radius a [27].

The linear dashed line describes the behavior of a particle in three-dimensions. The SD model is the curved dashed line with a logarithmic fall off of the reduced mobility given by $ln\frac{2}{\epsilon} - \gamma$. The experimental data in between these two regions confirms the extensions of the SD model. The crossover region curve will be referred to as the HPW plot for simplicity even though PS contributed to this result as well. These isolated island cases provide an experimentally confirmed comparison mechanism for the crowding experiment.

2.2 Two-Mutually Interacting Islands

Again, it is emphasized that the HPW and PS extensions to the SD model are only for *isolated* islands. The mobility of an island that is very crowded by neighboring islands is less understood due to the complexity of the mutual interactions. However, a pair of mutually interacting islands in 8CB films have been experimentally studied and theoretically corroborated in our lab [18]. The Saffman length is measured from the edge of the island and nearest crowding neighbors are other islands within this Saffman circle. Understanding mutual interactions is thus critical when studying the effects of crowding on the mobility of an island.

A pair of mutually interacting islands of radii a and b experiencing externally applied forces $\mathbf{F}_1$ and $\mathbf{F}_2$ have negligible inertial effects because the islands are in the low Reynolds number regime. These two islands are illustrated in Figure 2.2.

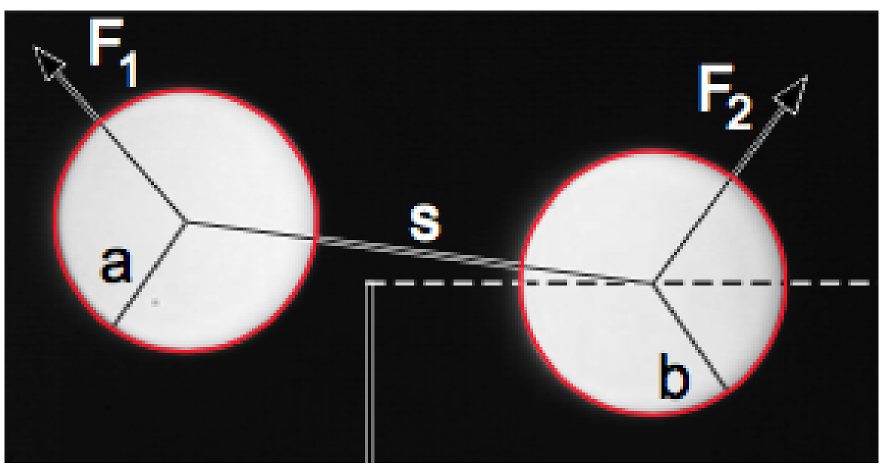

Figure 2.2: Two islands interacting with radii a and b. The centers of the islands are connected by the line s and each is experiencing an external force F [18].

The velocity of each island is dependent on its self-mobility and the mutual mobility with the other island. Equation 2.8 is the velocities for the two interacting islands. The self-mobility matrix is $\mathbf{M}_{11}$ and the mutual mobility is $\mathbf{M}_{12}$.

$$\mathbf{V}_1 = \mathbf{M}_{11}\mathbf{F}_1 + \mathbf{M}_{12}\mathbf{F}_2 \qquad \mathbf{V}_2 = \mathbf{M}_{11}\mathbf{F}_1 + \mathbf{M}_{12}\mathbf{F}_2 \tag{2.8}$$

A line connecting the centers of the two islands provides mirror symmetry and only the diagonal elements of the mobility matrix are non-vanishing. These diagonal elements are M_{11}^{rr}, $M_{11}^{\theta\theta}$, M_{12}^{rr} and $M_{12}^{\theta\theta}$ and are the self and mutual mobilities for the radial motion and the tangential motion denoted by rr and $\theta\theta$ respectively [18]. The cross-correlation function in Equation 2.9 below enables the mutual mobilities to be extracted from the experimentally measured mean-squared displacements. The displacement of the k^{th} island is given by $\Delta\mathbf{r}_k(t) = \mathbf{r}_k(t) - \mathbf{r}_k(0)$ in the time interval t. The initial distance between the islands is $r_{12}(0)$ at time t is s and the initial distance.

$$\langle \Delta\mathbf{r}_1(t) \cdot \Delta\mathbf{r}_2(t)\delta(r_{12}(0) - s)\rangle = 2k_BT(M_{11}^{rr}(s) + M_{12}^{\theta\theta}(s))t \tag{2.9}$$

For two islands of approximately equal radii that are less than the Saffman length for the film, the mobilities were found to be independent of the islands' radii. Furthermore, as the distance between the interacting islands decreased the mutual and self mobilities increased. Figure 2.3 is for pairs of oil droplets with radii $a \approx b < l_s$ on 8CB films.

For two islands with approximately equal radii that is greater than the Saffman length only the parallel component of the mobility was independent of the islands' radii, while the perpendicular component significantly depended on the islands' radii (Figure 2.4). When two interacting islands are of different radii, then the mobility depends on their size at all Saffman lengths.

In the highly crowded island system, the effects of nearest neighbors on an island's self mobility is of interest. Unlike the two-interacting island case, the mutual mobilities between the island of interest and all of its nearest neighbors cannot be extracted using the experimentally measured mean-squared displacements. Also, quantizing the effects of neighboring island interactions depends

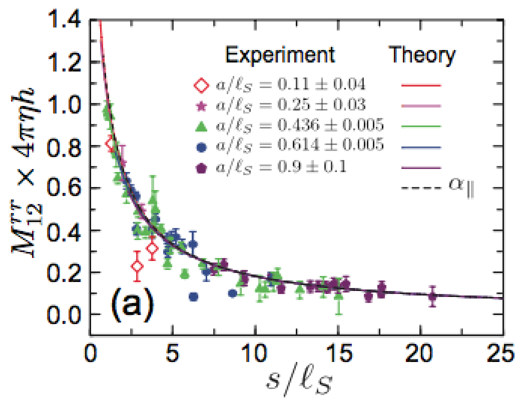

(a) radial

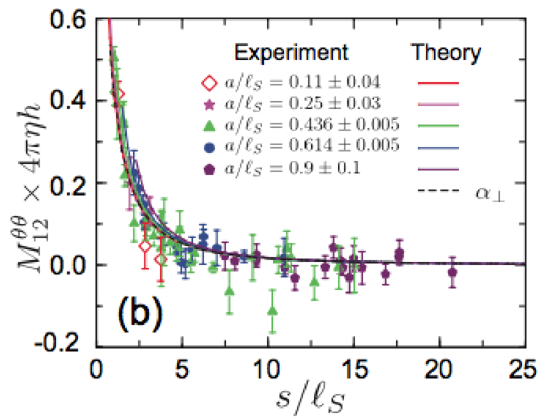

(b) tangential

Figure 2.3: Mutual mobilities versus reduced separation distance s/l_s of two interacting islands where $a \approx b < l_s$ [18]. (a) The radial component of the mutual mobility. (b) The tangential component of the mutual mobility.

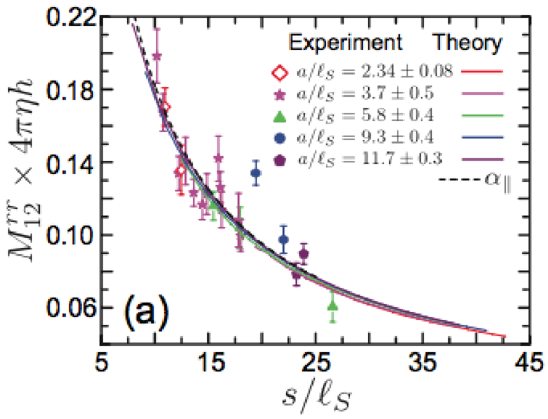

(a) radial

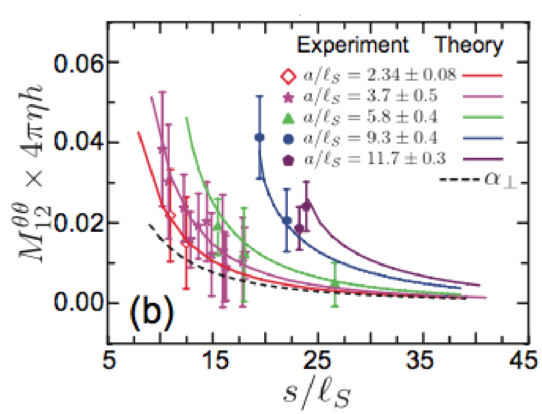

(b) tangential

Figure 2.4: Mutual mobilities versus reduced separation distance s/l_s of two interacting islands where $a \approx b > l_s$ [18]. (a) The radial component of the mutual mobility. (b) The tangential component of the mutual mobility.

greatly on the radii, separation distance and the Saffman length. Since the islands are more often of different radii than of the same, this complicates matters. Furthermore, each island of interest has a different environment of neighboring islands.

2.3 Tilt Experiment Theory

Unlike the crowding experiment, the theory underlying the tilting film experiment is well developed [28]. The motivation of the tilting film experiment is to study the mutual and self mobilities of islands with exactly equal radii when an external force is applied. Gravity is the simplest method for applying an external force. All that is required is tilting the film at a known angle. This is a simple “block on an incline” problem where the force **F** is the unknown quantity as depicted in Figure 2.5.

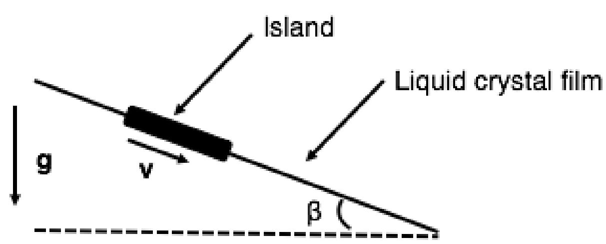

Figure 2.5: The tilt experiment is essentially a “block-on-an-incline” problem where β is the incline angle, **g** is gravity, and **v** is the velocity of the island traveling down the inclined film.

The fluid flow in the two-dimensional films satisfies the quasi-static Stokes equations and incompressibility conditions in equations 2.10 and2.11 below [28].

$$\eta_m \nabla^2 \mathbf{v} = \nabla p \tag{2.10}$$

$$\nabla \cdot \mathbf{v} = 0 \tag{2.11}$$

These equations are analogous to the image charge problems found in electrostatics. Image charge problems involve a charge near an infinite conducting plane that has a potential equal to $0V$. The potential or the electric field everywhere is found by imagining an image charge equal distance from the conductor on the other side. The two equal charges have electric field lines that cancel each other and thus the zero potential boundary condition is satisfied.

Similarly, a mirror island on the other side of the boundary wall has a fluid flow velocity field that cancels with the real island's velocity field and the boundary condition that the fluid does not flow along the edge of the boundary (no-slip condition) is satisfied. The tilt experiment provides the force and the method of reflections enables the mutual mobilities between the real island and its mirror island to be determined. Two cases are of interest. The first is the mutual interaction between two islands that are moving parallel to each other in the direction of the applied force. The second case is the mutual interaction between two islands moving towards each other. They are known as the parallel case and the perpendicular case respectively (Figure 2.6).

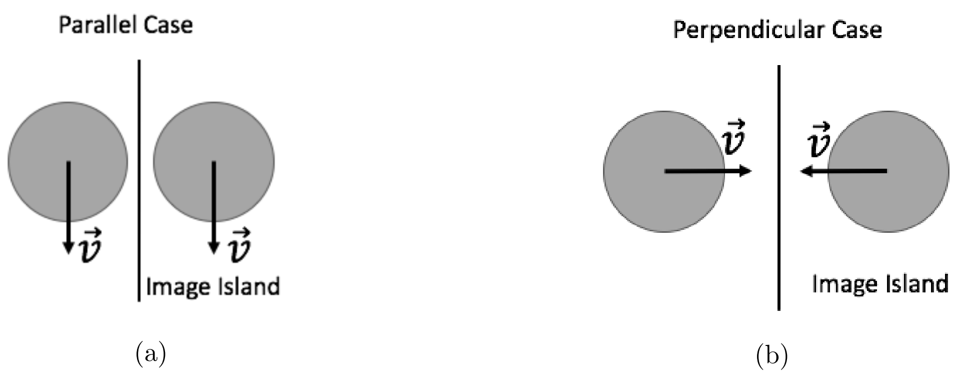

Figure 2.6: (a) The real island on the left is traveling parallel to the boundary illustrated as the black line. The image island is on the right of the boundary. (b) The real island is traveling perpendicular to the boundary and the image island is on the right.

Chapter 3

Experimental Methods

Smectic films are easily observed using reflected light microscopy. Two different microscopes were used for the tilted film and crowding experiments. The two-dimensional hydrodynamics of islands are measured by recording videos of the islands and tracking their motion. This chapter describes the apparatuses used and the methods of creating and tracking islands. The details of how the diffusion coefficient (in the case of the crowding experiment) and the mobility (in the case of the tilting film experiment) are extracted from data are also included in this chapter.

3.1 Experimental Apparatus and Reflected Light Microscopy

The Nikon Optiphot microscope was used primarily to collect data for the tilting film experiment, however, data for the crowding experiment was also collected. The objectives used for the tilted film experiment had magnifications of 5x and 10x while for the crowding data collected on this microscope had magnifications of 10x, 20x and 40x. The different objectives were easily switched between while collecting data using the turret attached to the microscope with four objective mounts. This microscope uses an incandescent light for the illumination source for the reflected light microscopy of the islands in the films.

A beam splitter directs light from the lamp through the objective and onto the film-holder. The light is then reflected off the islands into the CCD camera. Islands that are less than 20 layers thick appear gray while thicker islands have thicknesses comparable to the wavelengths of visible light and thus the islands appear in interference colors. The film holder is attached to a rotating translation stage which allows a region of interest to be viewed in the microscope. Figure 3.1 shows the Nikon microscope as well as a schematic of the light path.

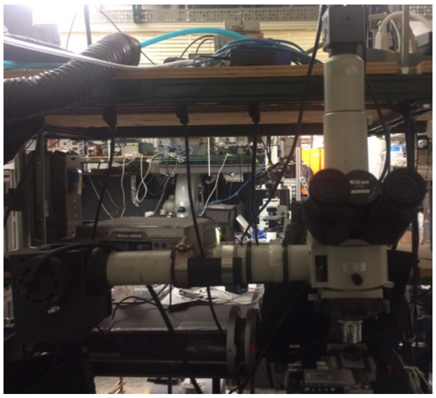

(a)

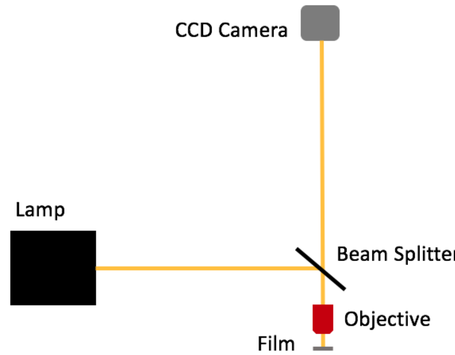

(b)

Figure 3.1: (a) Tilt experiment reflected light microscopy setup. (b) The corresponding light path for this microscope. Light originates at lamp, splitting at the beam splitter down through the objective and then reflecting off the film suspended in the film holder back up to the CCD camera.

This microscope is ideal for the tilted film experiment because it is attached to a device that tilts the entire apparatus by the turn of a handle in the x direction. The handle has degree measurement markings on it, however, the cycle of degree markings is only up to 90 degrees, so each full revolution has 4 of each degree marking. It is critical to record whether the handle is on the first, second, third, or fourth of the degree markings. Figure 3.2 is of the tilted apparatus with the handle included. The crowding data collected on this microscope is primarily a result of trying to create isolated islands necessary for the tilted film experiment, but getting a crowded system instead. Luck is crucial for collecting crowding data so rather than throwing out the data by popping the film, the tilt angle was locked at 0 degrees and crowding data was collected.

The CCD camera attached to the Nikon Optishot is a model WAT-221S Watec camera. This RGB camera has a resolution of 640x480 and runs at 24 fps. The film holder was a square piece

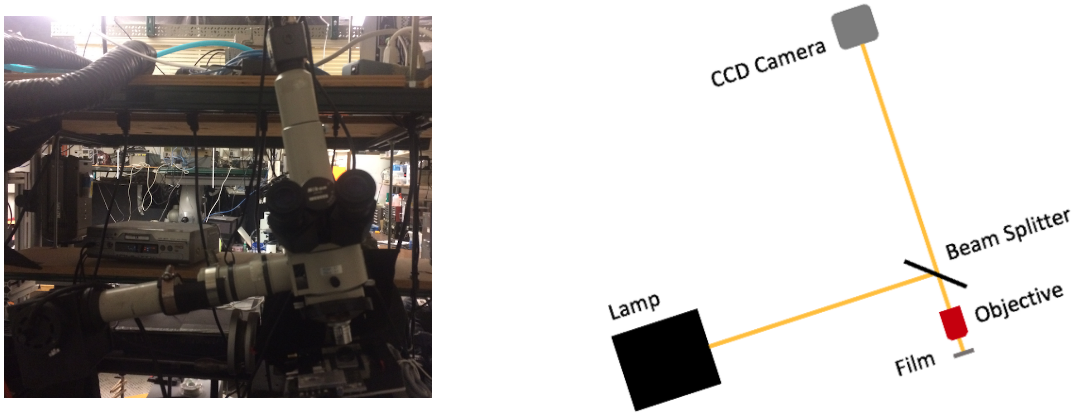

(a) (b)

Figure 3.2: (a) Tilt experiment reflected light microscopy setup tilted to an arbitrary angle. The tilt experiment does not require an extreme tilt angle as this, however such a degree demonstrates the utility of this setup. (b) The light path as explained in Figure 3.1 but now tilted to the same angle as the microscope.

of glass with a rectangular hole cut into it and then glued to an aluminum piece that attaches to the translational stage. I built an air shield by cutting a piece of plastic tubing at an angle and spray painting it black to minimize the amount of light reflected from the inside walls. Another square piece of glass without a hole drilled in it was then glued to the angle. The angle at which the air cover is cut at is crucial because if it is too low the glass cover piece will cause a very large glare on the film and the islands are then difficult to observe. If the angle is too high, then the microscope can't lower close enough to the film to resolve the picture. The air cover is placed on the film holder to cut out air flow above the film. Air flow below the film is also reduced because of the black cardboard that sits right under the film holder. The film holder, CCD camera and air cover are displayed in Figure 3.3.

The Olympus BX51 was the second microscope exclusively used for collecting crowded island data. The magnifications of the objectives used on this microscope were 5x, 20x, and 40x. This microscope also has a four objective turret that allows easy switching between the different

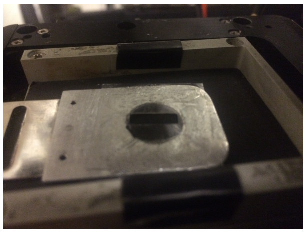

(a)

(b)

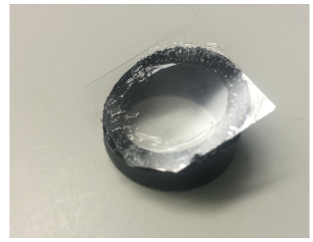

(c)

Figure 3.3: (a) Rectangular film holder for tilt experiment mounted on aluminum piece with circle drilled in through it and attached to translational stage. (b) Watec CCD camera model WAT-221S used attached to the tilt experiment microscope and computer used for recording. (c) Air cover for both the tilt and crowding experiments. This picture was taken intentionally with glare to better show the piece of glass.

objectives. The illumination system for the Olympus BX51 microscope is a 100 W Halogen light bulb. The light beam path is the same as the tilting film microscope in that a beam splitter directs the light from the lamp onto the film and then up into the CCD camera. Unlike the tilting film experiment, the crowding film holder is placed in the air chamber which has a hole drilled in the bottom of it. Figure 3.4 displays the microscope as well as a light beam schematic.

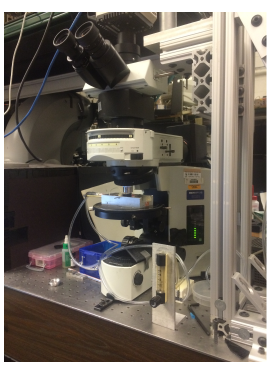

(a)

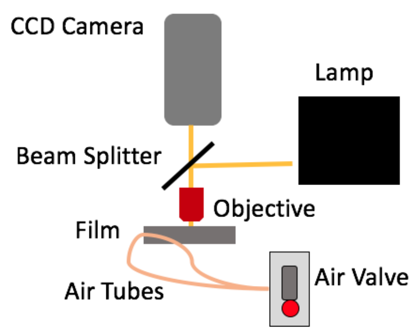

(b)

Figure 3.4: (a) Crowding experiment reflected light microscopy setup with air system. Note the CCD camera is not visible in this shot. (b) The corresponding light path for this microscope. Light originates at lamp and travels to the beam splitter where the light travels down through the objective and reflects back up to the CCD camera. The air valve controls the amount of nitrogen that travels through the air tubes and to the film holder.

The CCD camera used on this setup is the Memrecam GX-3 model V-190 and is attached to the microscope using the Olympus U-CMAD3 adapter. The resolution of this RGB camera is 1280 $\times$ 1024 and is set to its minimum frame rate of 50 fps. The same air cover is placed over the film holder to minimize the effects of air flow above the film. The air flow below the film is minimized by the air chamber. The CCD camera and film holder are displayed in Figure 3.5.

(a) (b)

Figure 3.5: (a) Crowding experiment circular film holder mounted on aluminum piece with a diameter of 1 cm. (b) GX-3 CCD camera model V-190 attached to crowding experiment microscope and computer used for recording. The air cover is the same as the one in Figure 3.3c.

3.2 Measuring Film Thickness

Different colors of islands are observed due to thin film reflection optics. This method of optical observation is also responsible for thinner regions of smectic material appearing black while thicker regions are very colorful. Constructive and destructive interference results from the light from the microscope reflecting off of the top as well as the bottom of the film it is incident upon. The distance between the reflective interfaces, in this case the top and bottom sides of the film, determines which wavelengths of the reflected light will interfere constructively or destructively. Thus, the thickness of the film and of the islands can be measured from the amount of reflected light.

The light from the microscope onto the film is at normal incidence and thus the reflectance only depends on the index of refraction of the surrounding air and of the 8CB comprising the film.

The air surrounding the film has an index of refraction equal to $n_{air} = 1$. The index of refraction for 8CB is equal to $n_{8CB} = 1.516$. The electromagnetic wave of the incident light is perpendicular to the director axis of the 8CB molecules. Since 8CB is in the smectic A phase the director axis is perpendicular to each layer. Thus, the reflectance is constant and given by equation 3.1.

$$r = \frac{n_{air} - n_{8CB}}{n_{air} + n_{8CB}} = \frac{1 - 1.516}{1 + 1.516} = -0.205 \tag{3.1}$$

The light incident on the top of the film acquires a 180° phase shift because the index of refraction of the 8CB reflection material is greater than the air incident material, i.e. $n_{8CB} > n_{air}$. The percentage of the reflectance reflected back when the light is incident on the bottom side of the thin film does not include this phase shift because the 8CB is now the incident material and the air is the reflected material, i.e. $n_{air} < n_{8CB}$. However, the light reflected from the bottom of the film acquires a phase shift when it is incident on the top of the thin film. This is because it has to travel the length of the film thickness twice and the light traveling in the 8CB material is moving slower than the light moving through the air due to the greater index of refraction for 8CB than air. The phase shift of the light that is reflected off the bottom of the film back up to the top is given by equation 3.2 where λ is the wavelength of the incident light and h is the film thickness. Since each film layer is quantized, then the film thickness h is equal to the length of the 8CB molecule times the number of layers.

$$\beta = \frac{2\pi n_{8CB} h}{\lambda} \tag{3.2}$$

The only unknown variables in the retardance equation above is the wavelength λ of the incident light and the thickness h of the region we are trying to measure whether this region is the film or an island. The double interference convolutes the calculation for the reflectivity so only the result is displayed in equation 3.3 where r again is the reflectance, β is the retardance and R is the reflectivity.

$$R = \frac{2r^2(1-\cos(2\beta))}{1-2r^2\cos(2\beta)+r^4} \tag{3.3}$$

A filter is attached to the microscope in order to separate the green light from the white light of the incandescent lamp. The wavelength λ is thus known, however, in order to solve for the film or island thickness h a known reflectivity R is necessary. Pieces of black glass are used in the lab for comparison due to its known property to reflect 4% of light incident on it. The relative intensities of the reflection from the black glass and from the film with **exactly** the same light settings and magnification are compared to determine the thickness h. The program ImageJ is very useful for measuring the relative intensities from images.

3.3 Calibrating the Microscopes

Converting the island measurements from pixels to microns requires the use of a reticule. This tool is a slide with a transparent circle in the middle where light transmits through with 100 division lines each a length of $0.1mm = 100\mu m$ on the transparent circle. Determining whether the camera has a square or a rectangular aspect ratio requires a picture taken both in the x and y directions. Below is a picture of what the reticule looks like under a 5x objective taken with the Gx Link camera.

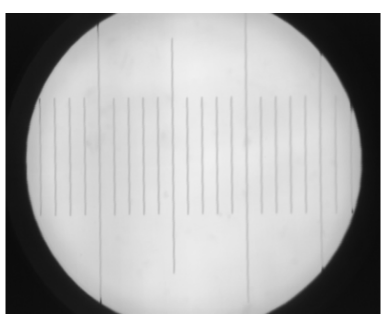

Figure 3.6: Reticule under a 5x objective and is used to find the conversion factor to convert measurements from pixels to microns. Each division is 100 μm and there are 100 division lines not all of which are visible here.

Measurements in the x and y directions must be made by placing the reticule perfectly with the division lines perpendicular to the axis being measured. This ensures consistency when later converting measurements in images. The conversion factor for each direction is determined by using the program ImageJ. The line tool is used to draw a line along the x or y axis and measured in units of pixels. The distance in μm is then divided by this pixel measurement to obtain a μm per pixel conversion. It is critical that the line drawn with the ImageJ tool starts either on the left of a division line and ends on the left of another division line or on the right and ends on the right. Below is a table for the tilt microscope camera (Watec Camera) and the crowding microscope camera (GX3 Link) 3.1.

Table 3.1: Table of conversion for the two cameras attached to the microscopes for the tilt (Watec camera) and crowding experiments (GX3 camera).

Objective	Watec ($\hat{x}$) (μ/px)	Watec ($\hat{y}$) (μ/px)	GX3($\hat{x} = \hat{y}$)† (μ/px)
5x	1.91	2.10	4.4
10x	0.917	1.00	2.10
20x	0.480	0.529	1.186
40x	0.243	0.265	0.589

† conversion in x direction is the same as the y direction for the GX3.

The crowding experiment camera has a square aspect ratio while the tilt camera has a rectangular aspect ratio. Whether the aspect ratio is square or rectangular does not matter. Each of the tracking programs described in the next sections have the ability to input the aspect ratios and output square images. In the case of the rectangular images, the y direction is converted to have the same conversion factor as the x direction. When the measurements of the islands need to be converted, now only the conversion for the x direction is needed.

3.4 Crowding Experiment

The process for collecting data for a film system with crowded islands involves multiple steps. First, the film must be drawn over the film holder and the air system must be set up so to create the crowded island system. This is done by positioning the film holder between the retractable needles through which the nitrogen flows. The air is adjusted until an ideal amount of liquid crystal material is blown onto the film. This usually takes a couple of tries. Once a desirable number of islands is achieved then the air cover must carefully be placed over the film without creating too much air flow or popping the film. The film must then be allowed time to settle so the fluid flow from the creation of the islands does not add additional movement to each island. Additional fluid flow may skew the mean-squared displacement measurements. Settling of the islands usually only takes a couple of minutes and provides the system to coalesce and reach a stable island environment.

At this time the GxLink computer software is opened on the computer attached to the microscope camera. In the software, the appropriate camera is then selected. When I collected data only the GxLink camera was connected to the microscope. This removed unintentional ambiguity that can arise from selecting the wrong camera and then using the wrong conversion factor.

The frames per second (fps) on the GxLink software is set to 50 fps. Record is then hit and a video of the system of islands is created. The videos from this software can be at most 3 minutes long. This is rather unfortunate because each video must be downloaded before another video can be created, otherwise the previous video is recorded over. Downloading can take up to 10 minutes which is enough time for islands to coalesce or for the film to pop. Since creating a high density island system is non-trivial, this downloading time can cost a lot of potential data. Often the high density system films are stable enough for a couple of videos to be taken before all of the islands diffuse back into the meniscus or into the film.

Another inconvenient event happens when the film is disturbed too much with the air flow and the entire meniscus is pushed onto the film. This results in a very thick, colorful, oily looking film where islands cannot be created and any amount of time waited does not yield the meniscus drifting back to the sides of the film holder. When this happens, it is best to pop the film and start again. Below are two ideal crowded systems 3.7.

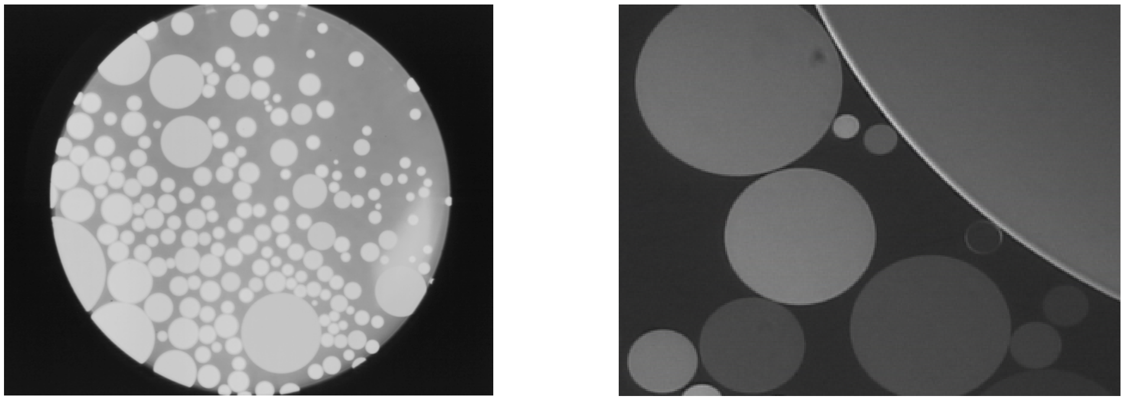

(a) (b)

Figure 3.7: (a) Crowded film with numerous islands of comparable size. (b) Large islands create a corral for smaller islands.

3.4.1 Tracking Islands

In order to calculate the diffusion coefficient for an island, the mean-squared displacement must be measured for each frame. This is achieved by using the IDL program TrackIsland.pro developed by Professor MacLennan to track the x and y coordinates of the center of the island of interest which corresponds to center of mass of the island because of its uniform density.

VideoMach is the software used to convert the videos of the islands to sequences of images. ImageJ is then used to find the appropriate threshold level that provides a high contrast between the island and the film. The threshold value is used to filter points that have intensity values above and below it. Any pixel with an intensity above the threshold is set to 255 and any pixel intensity below is set to 0. Thus, the final image is of a white island on a black film.

Finding the correct threshold level is achieved by either using the thresholding tool or by using the thresholding plot tool on the first image in the sequence. TrackIsland.pro also determines the average radius size of the island so it is critical that the threshold level is set in such a way that the true radius is not lost. If the video of the island, and hence the corresponding sequence of images is in color, then the image must be made composite in ImageJ to the grayscale. Figure 3.8 compares the actual image of an island to the images achieved by using a good threshold level and a bad threshold level.

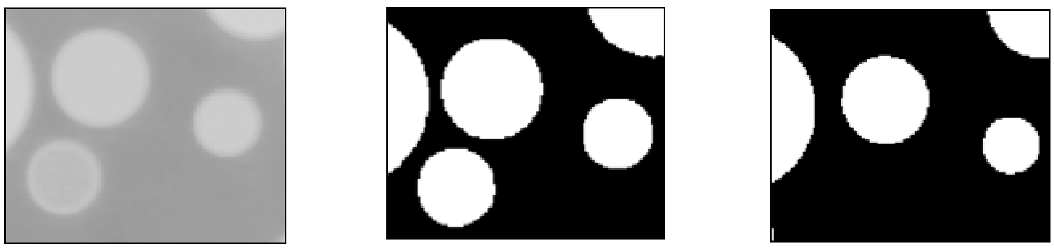

(a) Original image of islands. (b) Good threshold level. (c) Bad threshold level.

Figure 3.8: (a) Cropped image of 3 islands without thresholding. (b) Same three islands with correct thresholding where the radii of all three islands are preserved. (c) Incorrect thresholding results in disappearance of the middle island and the thresholded radii of the remaining islands are smaller than the in the original picture.

Finding the center of the islands of interest involves fitting an ellipse to the boundary of the island. The user sets the seed coordinates in the first thresholded image by clicking on it with the computer mouse or by setting the seed coordinates in the command file called "commands_droplets.pro". The intensity of this point is found and the surrounding region with the same intensity level is filled until the edge of the island is detected. The boundary of the island is detected because the intensity of the island is 255 while the intensity of the film is 0. Clicking on exactly the center is not necessary because the program calculates where the center is in the rest of the images. TrackIslands.pro then fits the island with an ellipse and outputs the coordinates of the center automatically for the entire sequence of images that are being analyzed. The camera corresponding to the data set can be set in the the commands to convert rectangular images to square images now with the conversion factor of the x direction.

TrackIsland.pro also has the capability to only analyze a cropped region, a very convenient tool when the island of interest takes up a very small region of the entire image. This also increases the speed of the program significantly; the smaller the region, the faster the program runs. The user can either input cropping coordinates in commands_droplets.pro or select the region with the mouse when prompted at the beginning of the program. Figure 3.9 shows the cropped analyzed region.

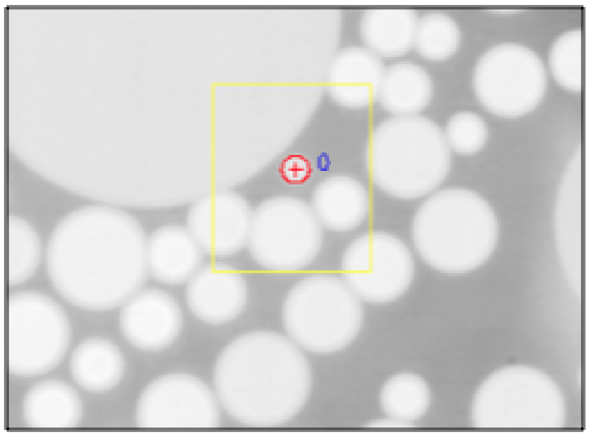

Figure 3.9: The yellow outlined box is the cropped region set in the IDL program diffusion.pro with the tracked island outlined with a red circle and marked with the blue number 0.

If the threshold of the island is not set correctly then the program loses the edge of the island and creates a much larger ellipse with the incorrect center and radius. When this happens the program must be stopped and the island must be reanalyzed with a different threshold level. The program will also lose the true center if the tracked island touches another island convoluting the true edge of the island. If the island drifts out of view then the center of the island is lost and TrackIslands.pro stops.

TrackIslands.pro outputs numerous files all of which contain the coordinates of the center of the island. Some of the files are in units of pixels while some are converted to units of millimeters. Some of the files output the radius of the island while others output the major and minor axes. The file I use for the next program to calculate the diffusion coefficient is the .epx file, which stands for “ellipse pixel”. This outputs the coordinates as well as the major and minor axes in units of pixels. Multiple islands can be tracked at once as seen in Figure 3.10, another convenient feature when analyzing a crowded system of islands. When multiple islands are tracked the output file bins the information for each island as seen in Figure 3.11. A typical input command as well as output file for this program is included in the appendix.

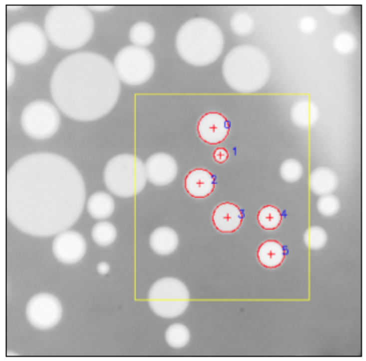

Figure 3.10: The yellow outlined box is the cropped region set in the IDL program diffusion.pro with six tracked islands outlined with red circles and marked with a blue number that is used to distinguish between the different islands in the diffusion.pro program.

```
File island.epx contains fitted ellipse information in pixel coordinates
time, {x[i], y[i], maj[i], min[i], o[i]} in pixels, degrees for all islands
```

Figure 3.11: Tracking program TrackIslands.pro output ".epx" file information for each column. The information in curly brackets repeats for each tracked island.

3.4.2 Measuring the Diffusion Coefficient

The goal of calculating the diffusion coefficient for systems of islands that are highly crowded is to compare the results to the theoretical HPW curve that is of reduced mobility versus reduced radius for isolated islands. This next section will describe how the diffusion coefficient is calculated using the IDL program called diffusion.pro and how each data point is plotted on the HPW curve using the IDL program called hpw.pro which is called by the command file plot_hpw.pro.

Diffusion_commands.pro calls the diffusion.pro program where the .epx ASCII file for the coordinates of the center of the island per frame is then analyzed. The user inputs the number of the frames to be analyzed as well as the number of frames per bin (time lag), the frame rate, the pixel to micron conversion factor in the x direction and the island number. For instance, the default island number for a single island is $myisland = 0$. If there are multiple islands, 5 islands for instance, then the 5^{th} island is inputted as $myisland = 4$.

The number of lag times $nlags$ is the number of frames over which the mean-squared displacement is calculated. This value is typically set to $10-20\%$ of the number of total frames, so for a data set of 100 frames, $nlags = 10$. To achieve a calculated diffusion coefficient in metric units, the frame rate and the pixel to micron conversions are used to convert units from $px^2/frame$ to $\mu m^2/sec$.

Diffusion.pro outputs numerous graphs that provide insight into the diffusive behavior of the island. These include the island's tracked trajectory and the x and y displacement histograms. These histograms are fitted with a gaussian curve. For perfectly Brownian behavior the island's trajectory will look like a random walk in two-dimensions. Linear drift is easily observed in the islands trajectory. Figure 3.13 displays the x and y histograms fitted with gaussian curves as well as two island trajectories, one for Brownian behavior and one with linear drift.

As discussed in chapter 2, the diffusion coefficient is easily calculated from the slope of the mean-squared displacement versus lag time. Since the behavior in the x and y directions are Brownian and independent of one another, the diffusion coefficient can be calculated from the slope of the mean-squared displacement in either direction. Diffusion.pro outputs the diffusion coefficient calculated in both directions as well as the average of the two. For my analysis, I use the average diffusion coefficient when comparing to the HPW theory plot. The error in the diffusion coefficient is calculated from the error in the mean-squared displacement slopes by the Markwardt fitting procedure.

The mean-squared displacement is calculated by the external software by Eric Weeks (and

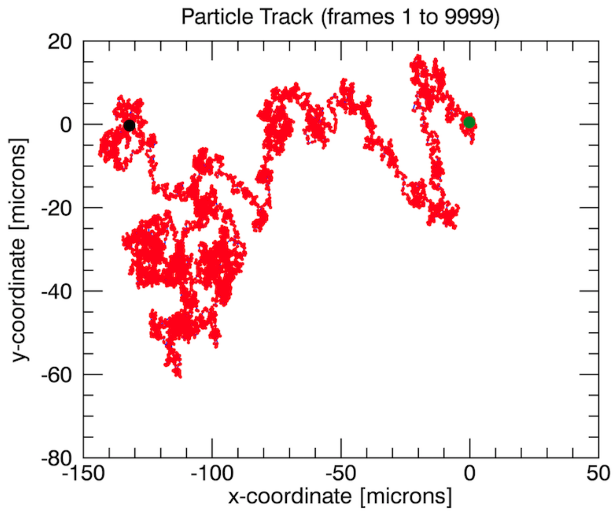

Figure 3.12: The IDL diffusion.pro output for a random two-dimensional walk particle tracking.

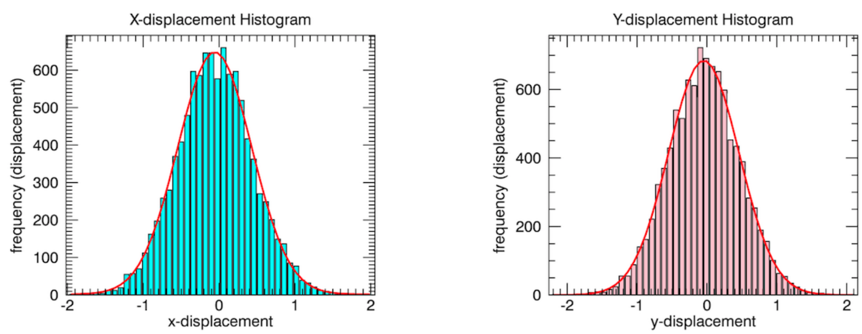

Figure 3.13: The IDL diffusion.pro output for a random two-dimensional walk with corresponding x and y displacement histograms.

thus is called the "Weeks method") [29]. This method gives an error bar to each experimental data point on the mean-squared displacement plot with an error corresponding to the number of frames that the mean-squared displacement was calculated over. For example, if I am analyzing a set of 100 frames (or images) with an $nlags = 10$, then all of the frames up to frame number 90 will have 10 frames over which the mean square displacement is averaged. The last 10 frames will have only the number of remaining frames to calculate the mean-squared displacement over, thus the last frame will have considerably more error because it will only have 1 frame to average the mean-squared displacement over. Figure3.14 displays the x and y mean-squared displacements for some data.

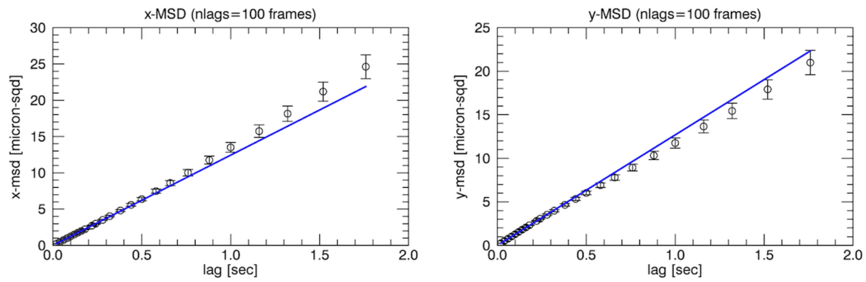

Figure 3.14: The IDL diffusion.pro output for random two-dimensional walk mean-square displacements in the x and y directions.

The hpw.pro IDL program is used once the diffusion coefficient, error on the diffusion coefficient, and the radius for a tracked island are calculated. Plot_hpw.pro is the command program which calls hpw.pro and where the user inputs the diffusion coefficient dc, the error err and the radius r as arrays for multiple islands. Since the reduced mobility and the reduced radius depend on the Saffman length, the thickness of the film is also entered as the array $nlayers$ of equal length to the other arrays.

3.5 Tilt Experiment

The process for collecting tilt data is similar to that of the crowding experiment. First, the film must be created on the film holder. Islands often form spontaneously on the film, but unlike the crowding experiment this system of sparse islands is ideal for the tilt experiment. When islands do not spontaneously form different methods can be used to create a few islands on the film without using the air system which generates too many islands. These include moving the air surrounding the film by waving a hand or by using a straw to gently blow air onto the film. Either of these methods are often enough to create a few islands. Once the islands are formed the air cover must be placed over the film holder to prevent further air flow around the film and to allow the fluid in the film to settle.

The x and y translational stage is then used to find an island that is in the same shot as the membrane edge. The rotational stage allows the film holder to be adjusted so that the film membrane lines up parallel with either the x or y axis depending on whether parallel or perpendicular data is being taken. Parallel data refers to capturing a video of an island traveling under the force of gravity parallel to the boundary a certain distance away from the membrane edge. Perpendicular data refers to when an island is moving under the force of gravity normal to the boundary.

In order to capture a video of the islands the television must be turned on and the eye piece rotated clockwise until the image viewed through the eyepiece of the microscope is viewed on the television. MovieMaker is the software used to record the video and unlike the GxLink software, can record data for up to 30 minutes. Once capture is selected on the software then the film is tilted the desired number of degrees. The tilting microscope was calibrated by using an electronic level and find the 0 degree measure which is at the 35 marking on the tilting microscope scale. The microscope was then tilted a quarter of a revolution to the 35 marking three additional times for one complete revolution and the degree measured by the level was recorded. From here the angle measurements were recorded at a full revolution five more times. This procedure was done for the microscope tilting left and tilting right.

3.5.1 Tracking Islands

Tracking islands with respect to the meniscus is very similar as the IDL program for the crowding experiment. First, the video of the island must be converted to a sequence of images and the correct threshold level must be determined from the first image. TrackIslandsEdge.pro requires that the islands be selected as well as the meniscus. A correct threshold level is one which maintains the correct radii for all of the islands and fills the entire boundary area. In order for the IDL code to know which contour corresponds to the boundary area it must be selected last. The islands and boundary area are filled as TrackIslands.pro does for the crowding experiment and are fitted with an ellipse. For simplicity I will continue to describe the program when only tracking one island.

A cyan line connects the center of the island with an initial guess to the edge of the boundary contour. The shortest distance normal to this edge is then calculated and plotted as a magenta line connecting the center of the island and the boundary. The program measures the length of this normal magenta line as a function of time and saves the output as the perpendicular distance. The program also saves the parallel distance the normal magenta line travels along the boundary contour. The final .epx file contains the frame number, the x and y coordinates for the center of the island, the parallel and perpendicular distances and finally the radius of the island.

3.5.2 Measuring the Mobility

Mobility was introduced in chapter 2 as the ratio of the velocity of the island with the external applied force $\mu = v_d/F$. The velocity is extracted perpendicular and parallel distances traveled with respect to the boundary edge per frame stored in the .epx file. These measurements are easily converted from $pixels/frame$ to m/s using the appropriate conversion factors for space and time. In MATLAB I used the "smooth" function to smooth the average velocity by averaging over 100 data points.

The force is calculated from the tilt angle as the case of the "block on an incline" problem. Once the force is known then using the velocity at each frame as the island approaches the boundary, the mobility is calculated. The reduced mobility is scaled by the constant $4\pi\eta_{8CB}h$ and the separation distance is scaled by the Saffman length ls.

Chapter 4

Data Analysis

4.1 Brownian Motion Simulation

I created a Brownian motion simulation in MATLAB as a verification of the IDL diffusion coefficient analyzing program diffusion.pro. The IDL code diffusion.pro calculates the diffusion coefficient two ways. The first is from the standard deviation σ of the fitted gaussian curves to the histograms for displacement in the x and y directions separately and then takes the average. The second method is from the slope of the mean-squared displacement versus time plots for each direction and then averages the two diffusion coefficients. The IDL program also subtracts off linear drift, an effect that is very common in experimental data.

The goal of the MATLAB Brownian motion simulation is to take a given diffusion coefficient as input and then generate a file of x and y coordinates for each frame that is then inputted into the diffusion.pro. Also, the Brownian motion simulation has the capacity to input linear drift. The simulation was developed using literature on the topic of simulating Brownian motion [30, 31, 32].

The simulation begins with user input prompts for the number of dimensions m, the number of frames n, the diffusion coefficient D, the frame rate fps, the amount of drift in the x direction $xDrift$ and in the y direction $yDrift$ and the number of time lags $nlags$. The simulation is also capable of creating data with a non-linear drift, however, any experimental data with non-linear drift (as is easily observed on the particle's track) is either not used, or broken into smaller segments where the drift is linear. As a result, only generated data completely without linear drift or with linear drift is of interest.

Brownian motion is a normal distribution of displacements. Creating the x and y coordinates utilizes the MATLAB function 'normrnd($\mu, \sigma, n, 1$)' which creates a column vector the length of the number of frames n that are of normally distributed random numbers with mean mu and standard deviation sigma.

Brownian motion is created by generating incremental x and y steps per frame. These are equal to $dx = normrnd(\mu, \sigma, n, 1)$ and $dy = normrnd(\mu, \sigma, n, 1)$. Linear drift is generated by adding on the $xDrift$ and $yDrift$ to each frame as follows: $dx = normrnd(\mu, \sigma, n, 1) + \sigma * xDrift$ and $dy = normrnd(\mu, \sigma, n, 1) + \sigma * yDrift$. Notice that the drift values are similarly given the correct units of μm by multiplying by the scaling factor $\sigma = \sqrt{2Ddt}$ where dt is the time per frame. In the case of no drift, the user simply inputs 0 for the values $xDrift$ and $yDrift$.

The x and y coordinates are created by taking the cumulative sum of the incremental steps corresponding to the direction, i.e. $x = cumsum(dx)$ and $y = cumsum(dy)$. The x and y vectors are then used to plot the random two-dimensional walk observed in the particle tracking. The incremental mean-squared displacement $dmsd$ is created by summing the squares of the incremental dx and dy steps. The total mean-square displacement msd is then the cumulative sum of the $dmsd$'s. The mean-square displacement versus frame is plotted using the cumulative sum of the $dmsd$. A linear polynomial fit is applied to the mean-squared displacement plot to find a fitted slope from which the diffusion coefficient is then calculated. The x and y displacement histograms are plotted from the incremental steps. A gaussian is fitted to both histogram and from these fits the standard deviation is calculated. The diffusion coefficient is related to the standard deviation by:

$$D = \sigma^2/(2 \times dt)$$

Figure 4.1 is the particle track of the simulated Brownian motion. The fitted histograms for the x and y displacements are in Figure 4.2 as well as the plot of the mean-squared displacement with the fitted linear slope. Figure 4.3 is the output from the simulation with the diffusion coefficients in units of $\mu m^2/s$ calculated from the x and y displacement histograms as well as from the mean-squared displacement slope. These calculated values for the diffusion coefficient are in close agreement with the inputted diffusion coefficient $D = 0.25\mu m^2/s$.

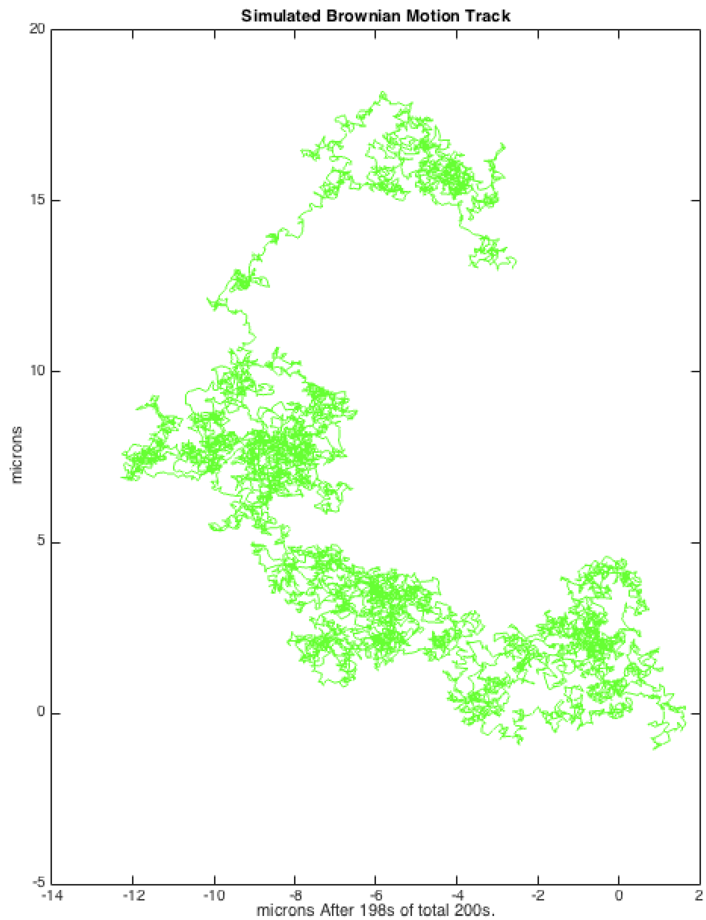

Figure 4.1: Simulated Brownian motion particle track for inputted diffusion coefficient $D = 0.25\mu m^2/s$ and no drift.

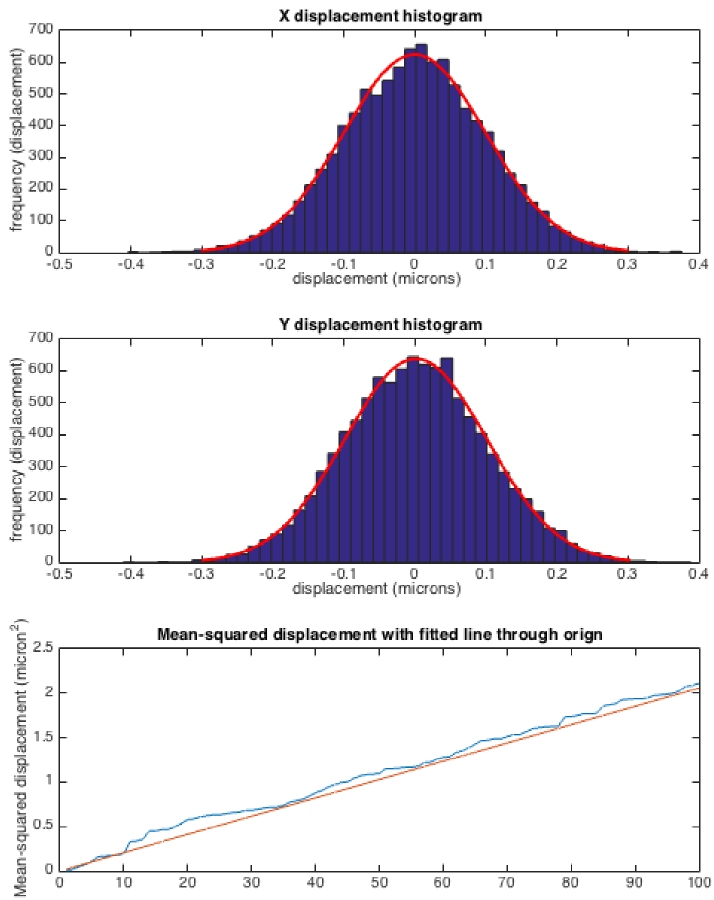

Figure 4.2: Brownian motion simulation x and y histograms with fit and the mean-squared displacement with linear fit for inputted diffusion coefficient $D = 0.25\mu m^2/s$ and no drift. The diffusion coefficient is recalculated by the simulation to ensure self-consistency.

```
sigma 0.1
 fps  50
dt 0.02
mean std var -0.00032958    0.099705   0.0099411
Dx = 0.24853
Dy = 0.2498
msd Slope 0.25714
```

Figure 4.3: Output from Brownian motion simulation includes the diffusion coefficient calculated from the standard deviation of the x and y displacement histograms as well as from the fitted slope for the mean-squared displacement plot.

4.2 Crowding Experiment Final Data

Oil droplets and islands were tracked using TrackIslands.pro to generate x and y coordinates saved to ".epx" files. The diffusion coefficients are determined by using the IDL program diffusion.pro with the "Weeks" method [29]. Each island track file generates one reduced mobility data point. The 40 reduced mobility data points against reduced radius are displayed in Figure 4.4.

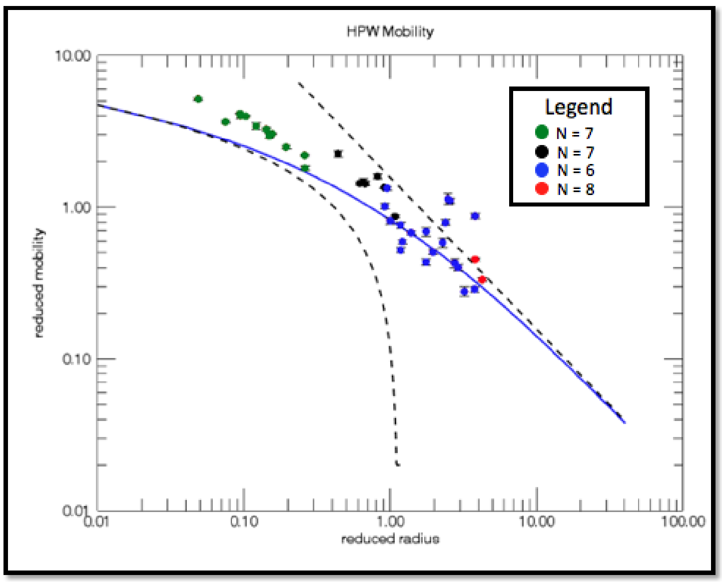

Figure 4.4: The reduced mobilities versus reduced radius for experimental data compared to HPW curve (blue line). The data consists of oil droplets (N = 7 green dots) and the rest are islands. The film thickness in number of layers for each data set is denoted by N.

Here the color code denotes the film thickness while also signaling the type of inclusion. The green data points are oil droplets on a seven layer film. The rest of the data points are islands on different film thicknesses.

4.3 Tilt Experiment Final Data

Data was collected for islands moving normal to the boundary, known as the perpendicular tilting film case, and for islands moving along side the boundary, known as the parallel tilting film case.

4.3.1 Perpendicular Tilting Film Case

Three different islands are analyzed for the perpendicular tilting film case. Each island is tracked using the TrackIslandEdge.pro. A line normal to the boundary from the center of the island determines the separation distance. The velocity of the island is determined from the rate at which this separation distance decreases as a function of time. Figure 4.5 portrays an island being tracked that is moving towards the boundary at different frame numbers.

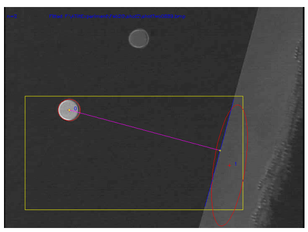

(a) Frame 002

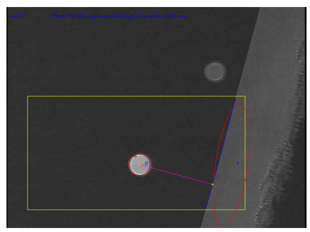

(b) Frame 375

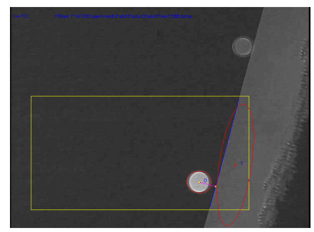

(c) Frame 701

Figure 4.5: Still frame progression of island moving perpendicular to boundary denoted by the frame number. The yellow box is the cropped region set by the tracking program. The magenta line measures the separation distance normal from the boundary to the center of the island. The red ellipse in the boundary is only used to find the edge of the boundary marked with a blue line.

The velocity as a function of time is very noisy as seen as the blue line data in Figure 4.6 for an island with reduced radius $a/l_s = 0.5847$. MATLAB's built in smoothing function "smooth" enabled the data to be averaged over a specified number of data points, in this case the average was over 100 data points. The smoothed velocity as seen as the red line in Figure 4.6 is the velocity used for the mobility calculation for the island.

The angle at which the film is tilted is used to determine the magnitude of the gravitational force applied to the island. Using the equation $\mu = v_d/F$ the mobility is easily determined. Recall, reduced mobility refers to the mobility μ multiplied by the constant $4\pi\eta_{8CB}h$. The reduced mobility corresponding to the island with reduced radius $a/l_s = 0.5847$ and corresponding to the velocity in

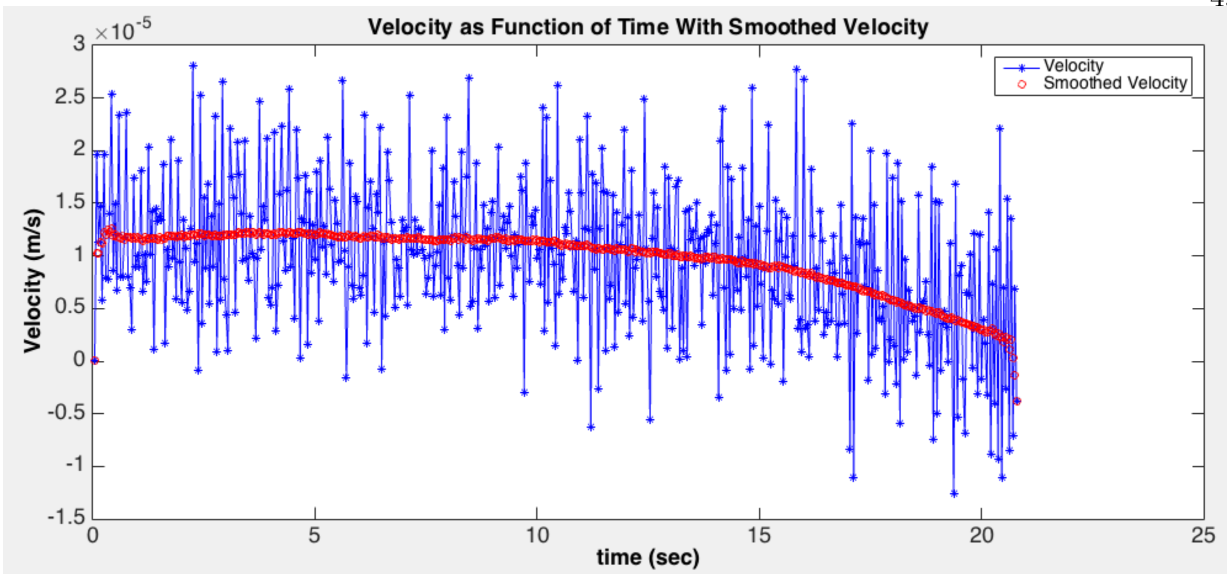

Figure 4.6: Velocity versus time for island moving perpendicular to boundary. The blue line is the raw velocity calculated from the change in separation distance per time. The smoothed velocity averages over 100 data points.

Figure 4.6 is portrayed in Figure 4.7.

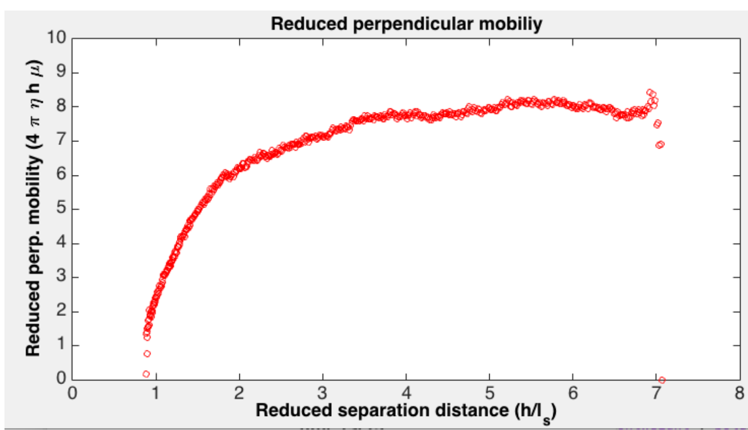

Figure 4.7: Reduced mobility as function of separation distance for island moving perpendicular to boundary corresponding to the data in Figure 4.6.

The x axis is the separation distance measured from the center of the island to the boundary in Saffman lengths. When the island is four to seven Saffman lengths away it levels off at a reduced mobility of about 8. As the island approaches the boundary it begins to have a smaller reduced mobility because the effect of the boundary is slowing the diffusion of the island. At a separation distance of two Saffman lengths, the island experiences its greatest decrease in mobility until the tracking stops right before the island hits the wall at less than one Saffman length away.

Figure 4.8 displays the theoretical curves developed by Dr. Tatiana Kuriabova and edited by John Papaioannou [28]. The experimental data for the reduced mobility for two of the islands is so much higher that it does not appear in the plot. Figure 4.9 better illustrates the scaled magnitude difference between the experimental data and the theoretical curves. This figure, however, is misleading for the largest perpendicular island in that the experimental data appears to land on the theory curve, when in fact it doesn't as evident in Figure 4.8.

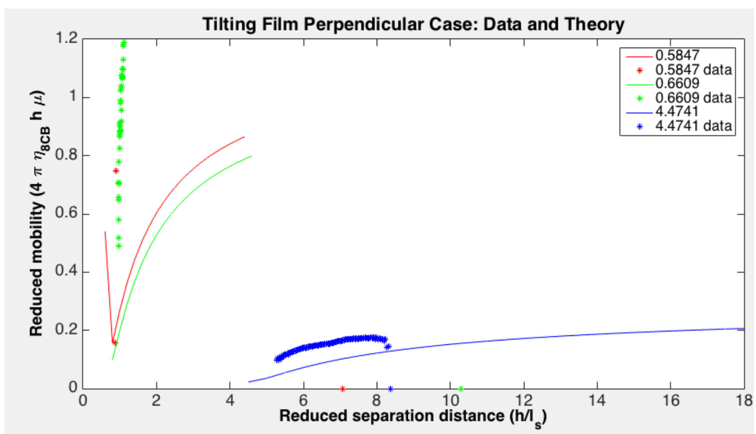

Figure 4.8: Zoomed in: Reduced mobility versus separation distance for islands moving perpendicular to boundary compared to theoretical curves. The theory curves are denoted with a straight line while the experimental data is denoted with star. Each data set and theory curve is labeled by the reduced radius a/l_s. The islands with reduced radius $a/l_s = 0.5847$ and $a/l_s = 0.6609$ were tilted at 3.4 degrees. The island with reduced radius $a/l_s = 4.4741$ was tilted at 7 degrees.

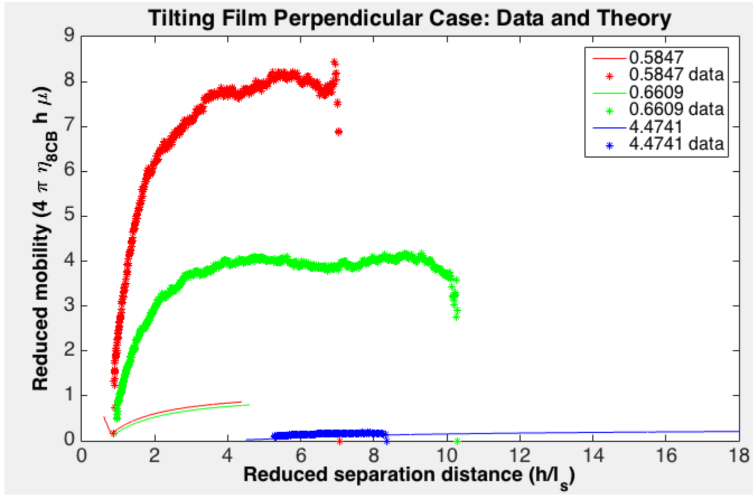

Figure 4.9: Zoomed out: Reduced mobility versus separation distance for islands moving perpendicular to boundary compared to theoretical curves. The theory curves are denoted with a straight line while the experimental data is denoted with star. Each data set and theory curve is labeled by the reduced radius a/l_s. The islands with reduced radius $a/l_s = 0.5847$ and $a/l_s = 0.6609$ were tilted at 3.4 degrees. The island with reduced radius $a/l_s = 4.4741$ was tilted at 7 degrees.

4.3.2 Parallel Tilting Film Case

There is a significant difference in the amount of data needed for the perpendicular tilting film case compared to the the parallel tilting film case. For each perpendicular run for a single island, an entire curve of reduced mobility versus separation distance experimental data is collected. On the other hand, for each parallel run for a single island a single data point is collected.

The data I collected for the parallel tilting film case consists of different islands all of different reduced radii at different separation distances. Many of the collected data were of islands drifting too close to the boundary for conclusive results. The interesting data points are those of islands that are more than a couple of pixels away from the boundary. Thus, the tilting film parallel case consists of seven different islands.

A line is fit to the boundary in TrackIslandEdge.pro so the line normal to the boundary from the center of the island traces a distance along the boundary line. The velocity of the island is determined from the distance traced by the connector line between the island and boundary along the boundary line as a function of time.

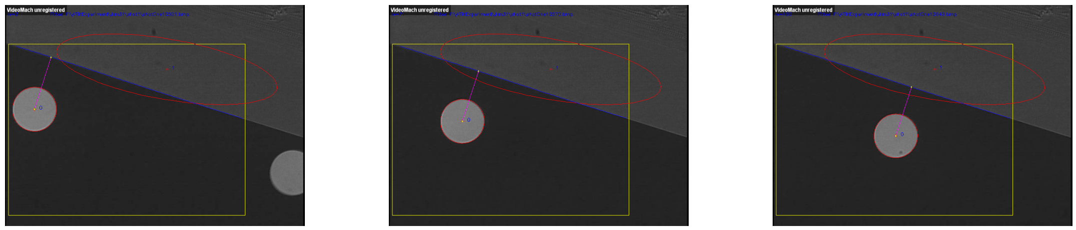

(a) Frame 002 (b) Frame 071 (c) Frame 150

Figure 4.10: Still frame progression of island moving parallel to boundary denoted by the frame number. The yellow box is the cropped region set by the tracking program. The magenta line measures the separation distance normal from the boundary to the center of the island. The red ellipse in the boundary is only used to find the edge of the boundary marked with a blue line.

The separation distance of the island is once again measured by the connector line. Figure 4.11 is the data for an island with reduced radius $a/l_s = 0.9829$ with the raw velocity as the blue line and the smoothed velocity as the red line.

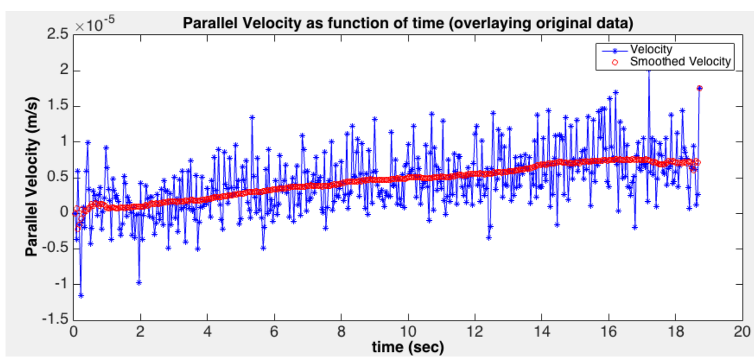

Figure 4.11: Velocity versus time for island moving parallel to boundary. The blue line is the raw velocity calculated from the change in separation distance per time. The smoothed velocity averages over 100 data points.

Here the reduced mobility is increasing as a function of time. The gravitational force the island experiences is once again calculated from the angle of the tilting film and the mobility is calculated from the smoothed velocity and the gravitational force. Since this plot translates to a single data point, the reduced mobility and separation distance compared to the theoretical curves is the average of the first 30 measurements. All of the theoretical curves are plotted in Figure 5.17 and the reduced mobility for the island with reduced radius $a/l_s = 0.9829$ discussed above is seen here. The rest of the experimental values for the reduced mobilities are shown in Figure 5.18.

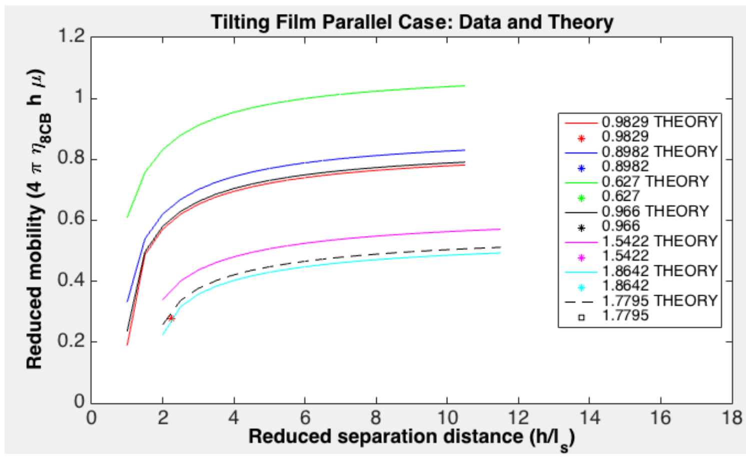

Figure 4.12: Zoomed in: Reduced mobility versus separation distance for islands moving parallel to boundary compared to theoretical curves. The theory curves are denoted with a straight line while the experimental data is denoted with star. Each data set and theory curve is labeled by the reduced radius a/l_s. All parallel case islands were tilted at 2.6 degrees.

The experimental reduced mobilities are significantly greater than the theoretical curves all but for the case where $a/l_s = 0.9892$. These results and their implications are discussed in the next chapter.

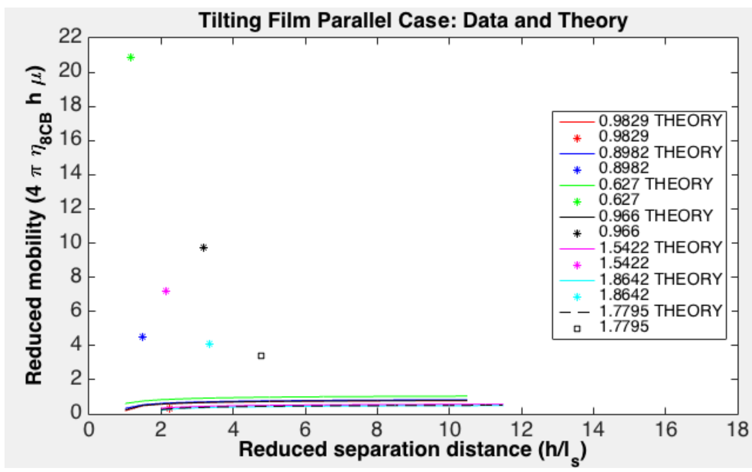

Figure 4.13: Zoomed out: Reduced mobility versus separation distance for islands moving parallel to boundary compared to theoretical curves. The theory curves are denoted with a straight line while the experimental data is denoted with star. Each data set and theory curve is labeled by the reduced radius a/l_s. All parallel case islands were tilted at 2.6 degrees.

Chapter 5

Results and Discussions

Chapter 4 introduced the results from the crowding experiment and the perpendicular and parallel cases for the tilting film experiment. This chapter discusses these results and provides insight to the underlying physics.

5.1 Crowding Experiment

According to the HPW theory, an isolated island of a given reduced radius has a maximum reduced mobility given by the blue curve in Figure 5.1. The results for the crowding experiment include the reduced mobilities for oil droplets and islands, however, a majority of the data points lie above the isolated island HPW curve in Figure 5.1. Here the oil droplets are all on the seven layer film labeled by the green dots. The rest of the data points are islands created by air on film thicknesses of six, seven and eight layers. In order to better understand the results in this plot, I have created four data point call outs. The first call out is for the largest oil droplet that has a reduced mobility and reduced radius such that the data point hits the isolated island HPW curve shown in Figure 5.2.

From the image of the island it is evident that this island is not completely isolated as is necessary for the HPW model. Furthermore, the x and y mean-squared displacement curves both have a roll over from the linear fit which is characteristic of confined Brownian motion. The particle

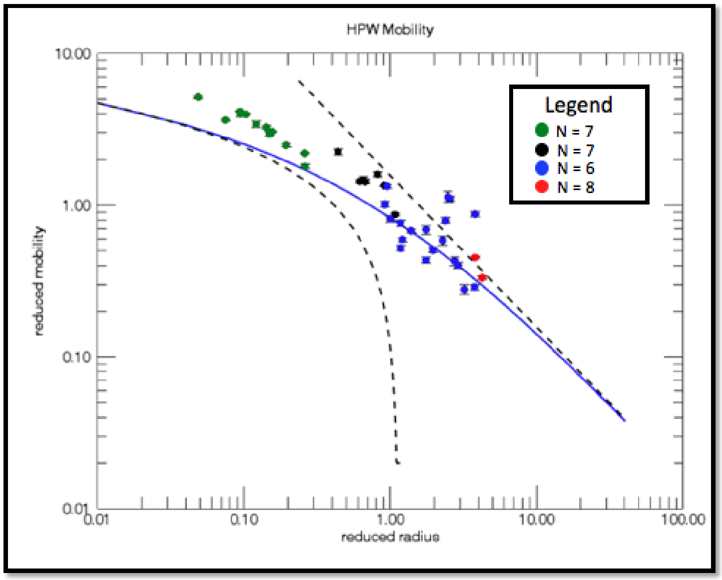

Figure 5.1: The reduced mobilities versus reduced radius for experimental data compared to HPW curve (blue line). The data consists of oil droplets (N = 7 green dots) and the rest are islands. The film thickness in number of layers for each data set is denoted by N.

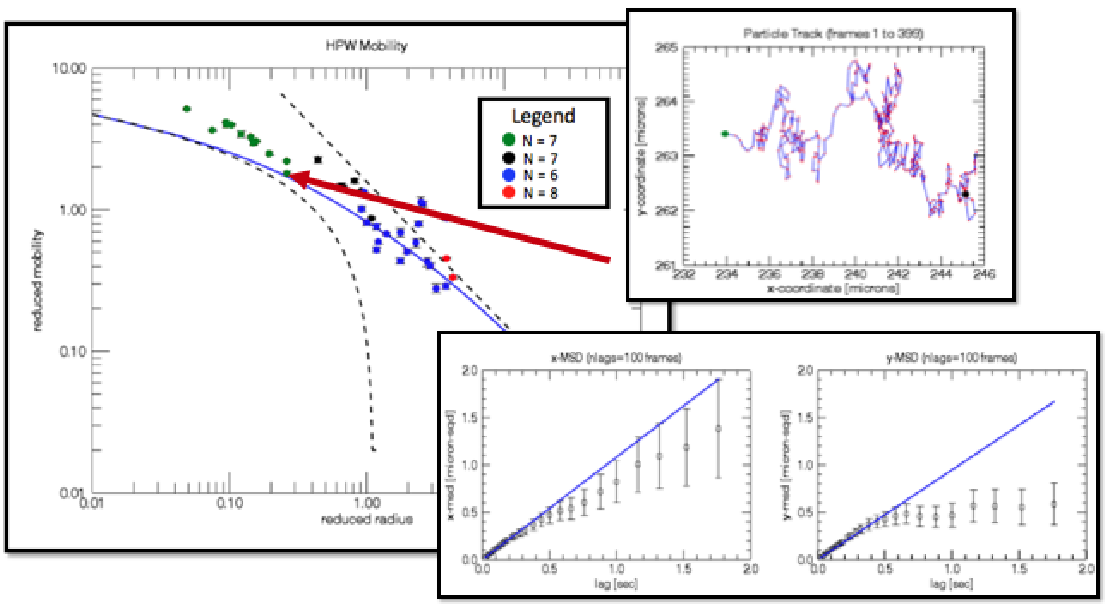

Figure 5.2: Largest oil droplet hits the isolated island HPW value. The particle tracking shows Brownian motion while the x and y mean-squared displacement plots show roll overs from linear fit characteristic of confinement.

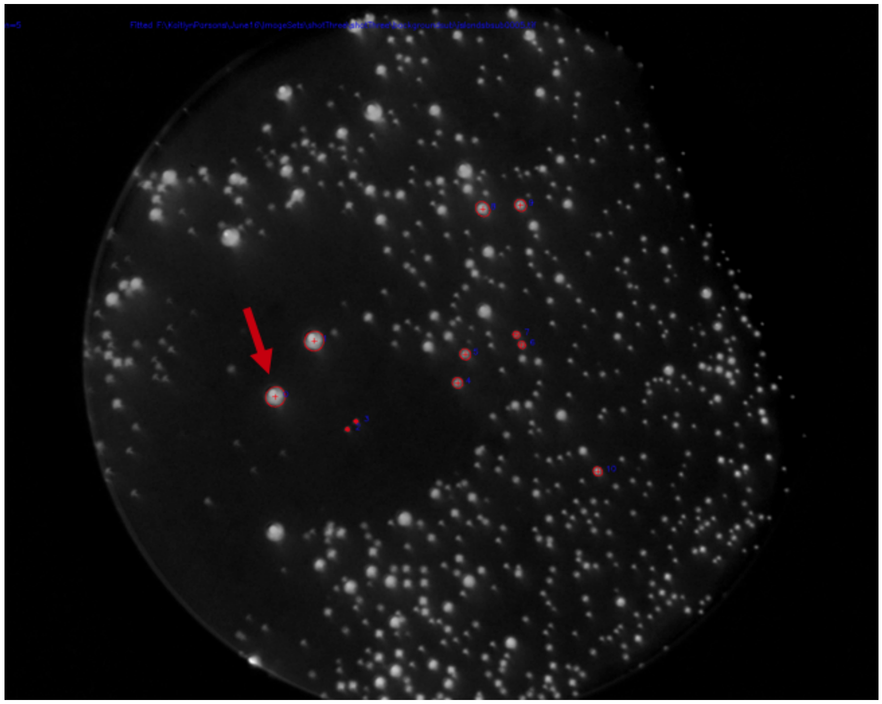

Figure 5.3: Corresponding film environment for call out number 1. A background shot was taken and then subtracted out of the original images which results in a very black film. Red arrow is pointing to the island corresponding to the data in Figure 5.2.

track for this oil droplet is very resemblant of Brownian motion. Possible drift would occur in the x direction, however, the amount of drift is small enough that the diffusion.pro program is able to accurately subtract it out.

The second call out is of one of the largest islands on a six layer film as seen in Figure 5.4. This data point also has a reduced mobility and reduced radius such that the data point hits the isolated island HPW curve. The mean-squared displacement in the x direction has the roll over effect characteristic of confinement, however, the mean-squared displacement in the y direction has a slope that increases faster than the fitted polynomial which I refer to as "super-linear". The particle track for this island shows that the displacement in the x direction is over a much smaller scale than the y direction. Thus, for this island, linear drift occurs more prominently in the y direction.

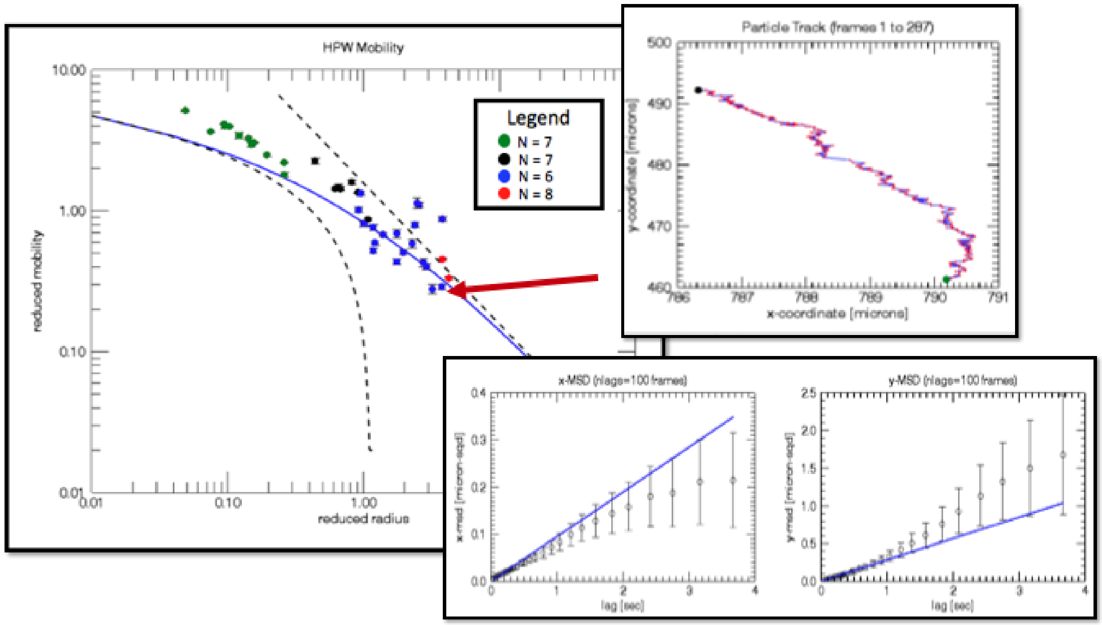

Figure 5.4: Largest island a little below the isolated island HPW value. The particle tracking shows Brownian motion in the x direction and linear drift in the y direction. The mean-squared displacement in x rolls over from the linear fit characteristic of confinement. The mean-squared displacement in y increases faster than the linear fit ("super-linear").

The third call out is of one of the largest islands on the six layer film as seen in Figure 5.6. This island has an experimentally measured reduced mobility that is 5 times greater than the isolated island HPW case with the same reduced radius. The reduced mobility is so much greater for this reduced radius that it even exceeds the three-dimensional model which is the top dashed line. The drift for this data point is significantly greater than the previous two call outs in both the x and y direction. The mean-squared displacement in the x direction begins with a slope increasing faster than the fitted linear slope, however, it begins to roll over at 2 seconds and then begins to linearly increase at 3 seconds. The mean-squared displacement in the y direction has a trend that is curving up and away from the fitted linear slope. Both of these mean-squared displacements are uncharacteristic of confinement or isolation.

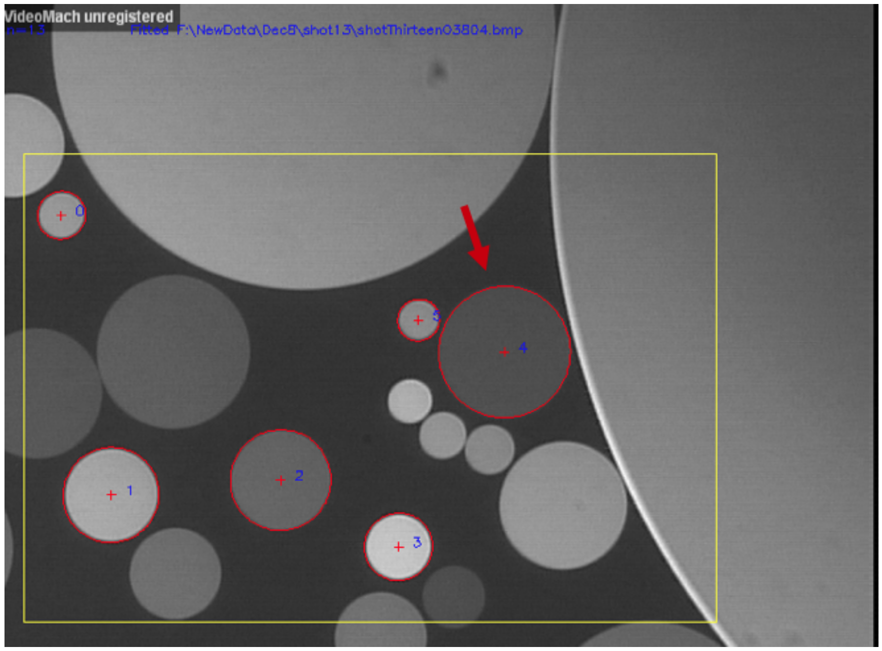

Figure 5.5: Corresponding film environment for call out number 2. Red arrow is pointing to the island corresponding to the data in Figure 5.4.

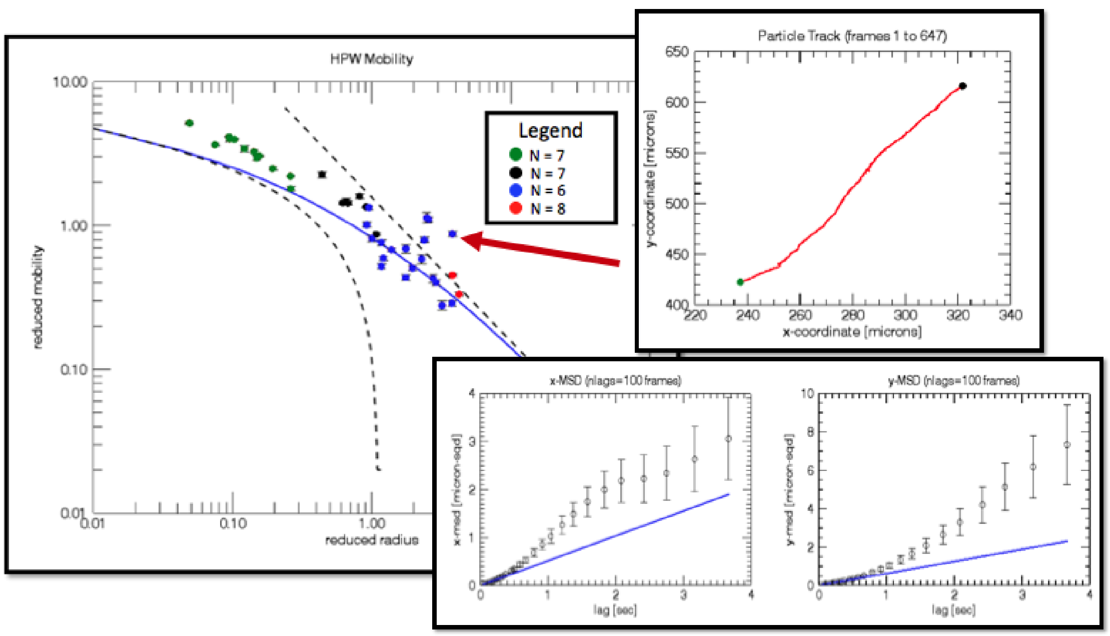

Figure 5.6: Another one of the largest islands above the isolated island HPW value. The particle tracking shows substantial linear drift in both directions and mean-squared displacements increasing faster than the linear fit ("super-linear").

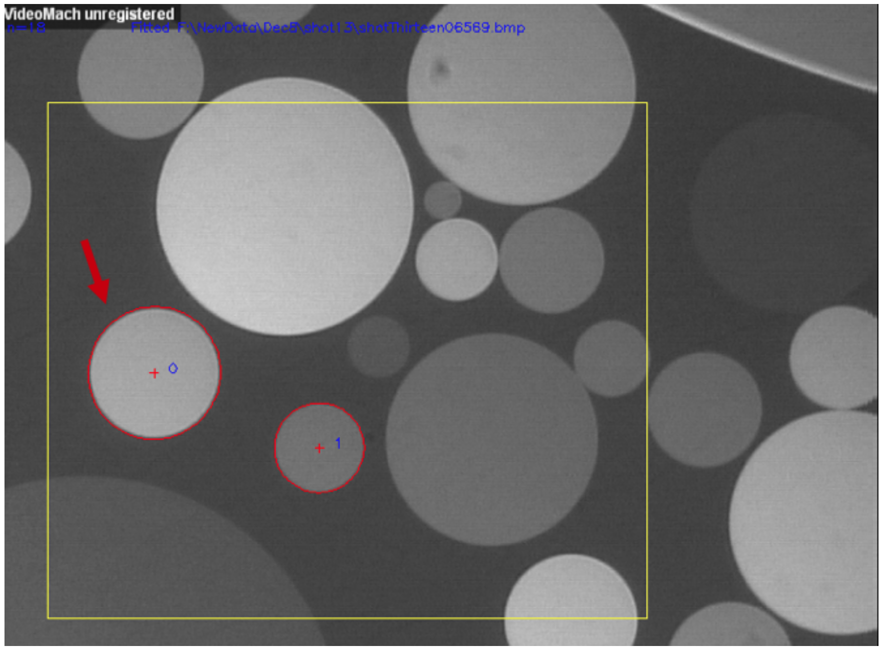

Figure 5.7: Corresponding film environment for call out number 3. Red arrow is pointing to the island corresponding to the data in Figure 5.6.

The final call out is of the smallest oil droplet with the largest reduced mobility on the seven layer film seen in Figure 5.8. The particle tracking for this oil droplet is Brownian with a small amount of drift in the x direction which the diffusion.pro program accurately subtracts out. The mean-squared displacements in the x and y directions both exhibit a roll over from the fitted linear polynomial. The mean-squared displacements indicate the oil droplet is confined in both directions and yet it has a reduced mobility 2 times higher than the isolated island HPW value. The picture of this oil droplet clearly indicates the island is not isolated.

Out of the four data points discussed above, the third data point discussed in Figure 5.6 has the most substantial linear drift in both directions as well as a "super-linear" mean-squared displacement in both directions. The y position change is $\Delta y = 200\mu m$ and the x position change is $\Delta x = 93\mu m$ which yields a total distance $\Delta r = 200.5\mu m$. The second data point discussed in Figure 5.4 has the second most substantial linear drift with $\Delta y = 32$, $\Delta x = 4\mu m$ yielding $\Delta r = 32.2\mu m$.

From these two data sets it is observed that when the displacement in the y direction is

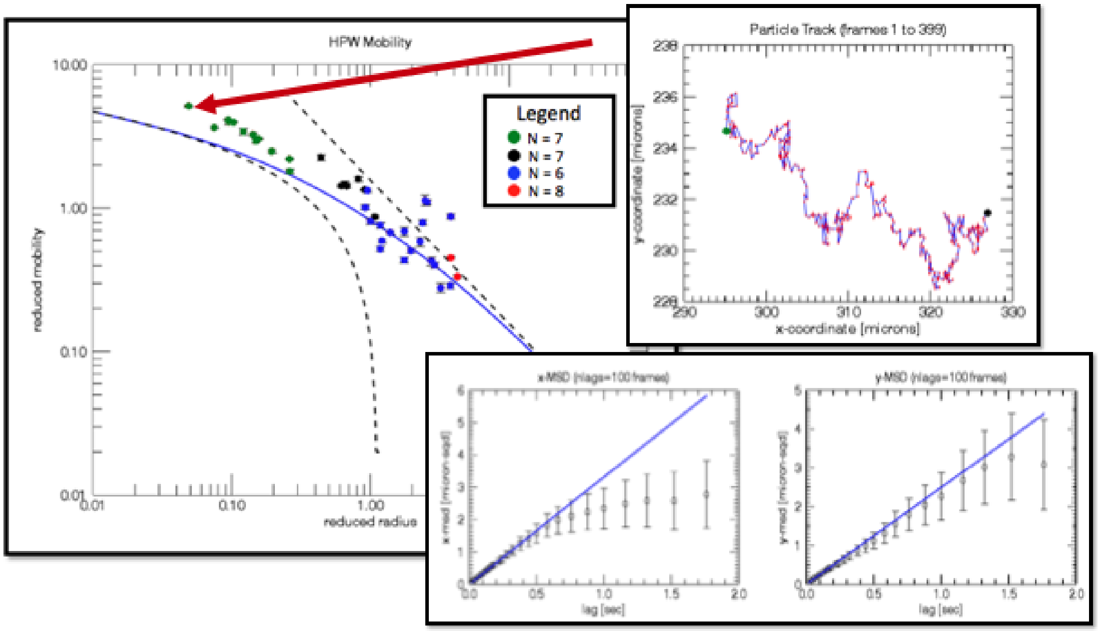

Figure 5.8: Smallest oil droplet above the isolated island HPW value. The particle tracking shows Brownian motion in the x and y directions. The mean-squared displacement in x and y roll over from the linear fit characteristic of confinement.

between 20 to 200 μm then the corresponding mean-squared displacement is also "super-linear". When the displacement in the x direction is greater than or equal to $90\mu m$, the corresponding mean-squared displacement is also "super-linear". It is not clear what is initiating the linear drift component in some islands and not others, perhaps fluid flow from pervious coalescence events in the film, for example. Diffusion.pro may need enhancement to remove substantial linear drift including handling linear drift in the x and y directions equally.

Now considering the first and fourth data points discussed above in Figures 5.2 and 5.8 respectively. Both data points have similar Brownian motion particle tracking and a roll over effect in both the x and y direction. The similar mean-squared displacement plots should indicate similar confinement effects. It is unclear why the fourth data point has a reduced mobility and reduced radius such that it hits the isolated island HPW curve value and the first data point has a reduced mobility 3 times greater than the isolated island HPW value.

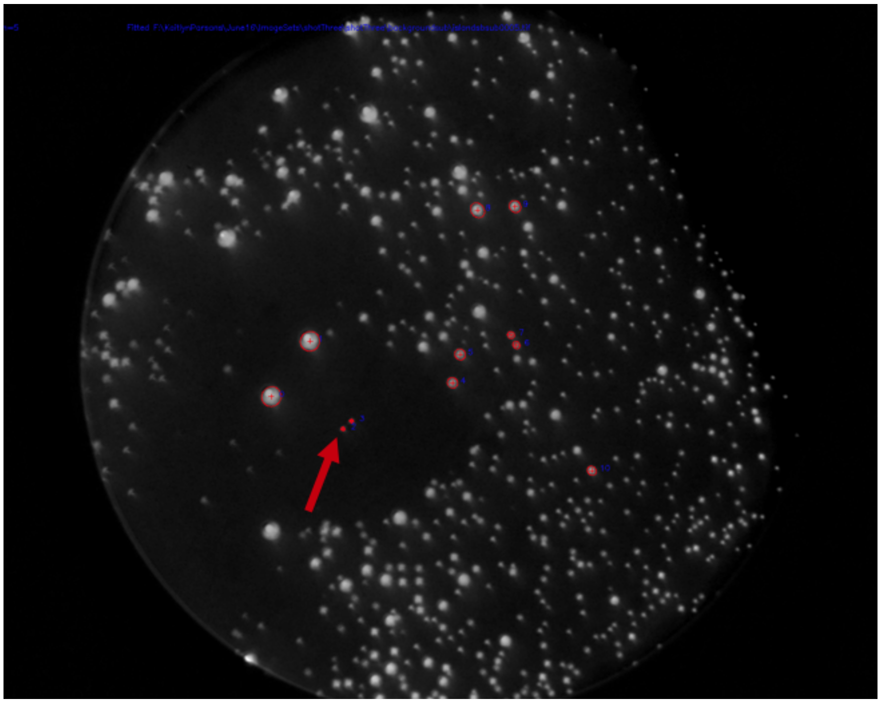

Figure 5.9: Corresponding film environment for call out number 1. This is the same film as call out number 1. Again, the background shot was subtracted out of the original images which results in a very black film. Red arrow is pointing to the island corresponding to the data in Figure 5.8.

5.2 Tilting Film Experiment: Perpendicular Case

Three islands moving perpendicular to the boundary are studied. Two of these islands, both on the same film, have reduced mobilities 4 and 8 times greater than the theoretical curves (and thus the HPW isolated island values). The third island has reduced mobility much closer to the theory curve. This third island, labeled by its reduced radius $a/l_s = 4.4741$, will be discussed first.

The island with reduced radius $a/l_s = 4.4741$ is on a film with a thickness of 7 layers tilted at 7 degrees from the horizontal, has a diameter of 308 pixels and the island is 10 layers thick. Figure 5.10 displays the island's velocity as a function time as the blue line and the smoothed velocity as the red line.

Here it is observed that the velocity measurements have a wide variance or deviation that

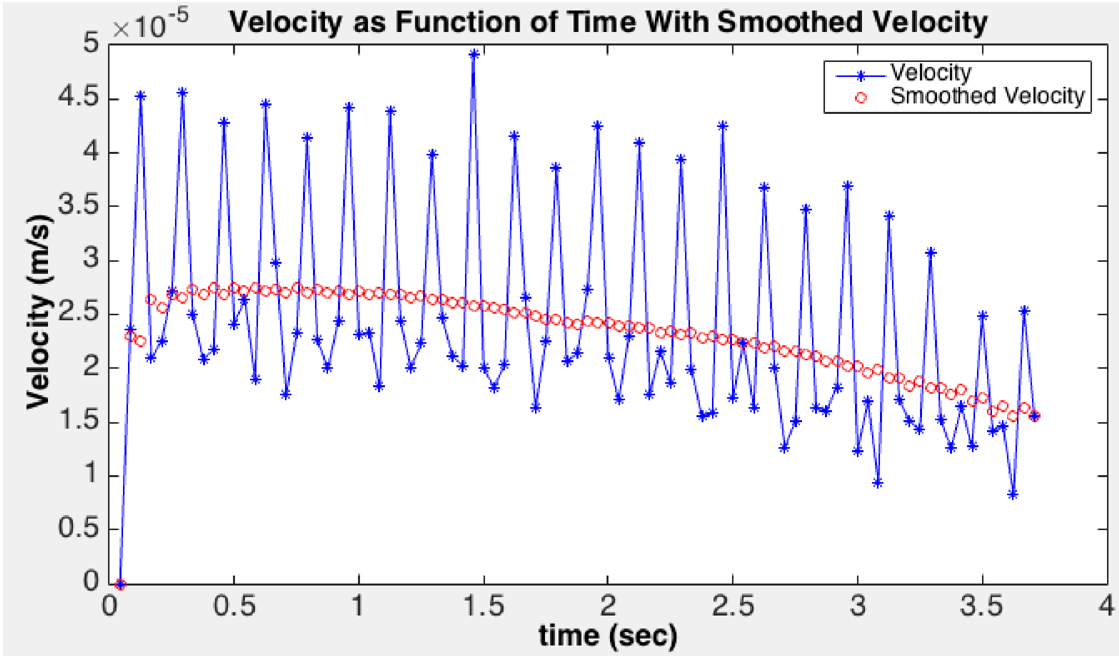

Figure 5.10: Velocity versus time for perpendicular moving island with reduced radius $a/l_s = 4.4741$ tilted at 7 degrees. The blue line is the raw velocity calculated from the change in separation distance per time. The smoothed velocity averages over 100 data points.

appears to have a periodic component. For every velocity data point around $4.5 \times 10^{-5} m/s$ there are three data points around $2.5 \times 10^{-5} m/s$. To remove this variance, the velocity data is low pass filtered with a running average over 100 data points. Figure 5.11 compares the reduced mobility of this island with the separation distance with the boundary. Here the island's velocity decreases as it approaches the boundary.

The next two islands, labeled by their reduced radius $a/l_s = 0.5847$ and $a/l_s = 0.6609$, are both on a 8 layer film and are of thicknesses of 10 and 15 layers and have diameters of 46 pixels and 52 pixels, respectively. This film is tilted at 3.4 degrees measured from the horizontal.

Figure 5.12 displays the velocity of the island with reduced radius $a/l_s = 0.5847$. Figure 5.13 displays the velocity of the island with reduced radius $a/l_s = 0.6609$. Again, the velocity is the blue line and the smoothed velocity is the red line.

Here the two islands of very close radii travel at about the same velocity of $1.1 \times 10^{-5} m/s$ and both slow down as they approach the boundary. Unlike the larger island with reduced radius

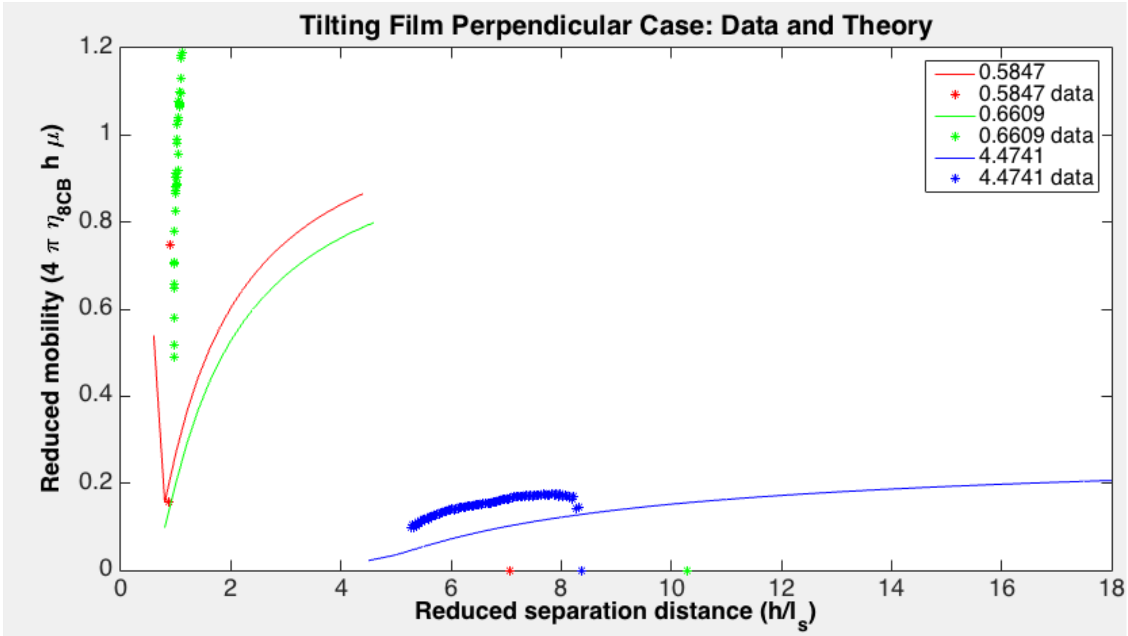

Figure 5.11: Reduced mobility for island with reduced radius $a/l_s = 4.4741$ scaled to compare to theory. Theory marked by solid lines while data marked by a star. The data for the other two islands is not visible on this scale (see Figure FinalPerpPlot2chap5).

$a/l_s = 4.4741$, these islands have reduced mobilities much greater than the theoretical curves as seen in Figure 5.14.

Both the island with reduced radius $a/l_s = 0.5847$ and the island with reduced radius $a/l_s = 0.6609$ have a hook on the data at the beginning of the track due to the smoothing of the velocity data. For the island with reduced radius $a/l_s = 0.5847$ the reduced mobility reaches an average level of 8 between the reduced separation distance of 5 to 8. This reduced mobility is 8 times greater than the theoretical curve of which saturates at great separation distances to the isolated island HPW value. At the separation distance of 4, the reduced mobility quickly decreases until the island is no longer tracked right before it hits the boundary at separation distance of 1. Similarly, the island with reduced radius $a/l_s = 0.6609$ has a level reduced mobility of 4 at reduced separation distances between 5 and 10. This reduced mobility is 4 times greater than the theoretical curve. Once the island reaches a separation distance of 4, the reduced mobility decreases until the island is no longer tracked right before it hits the wall.

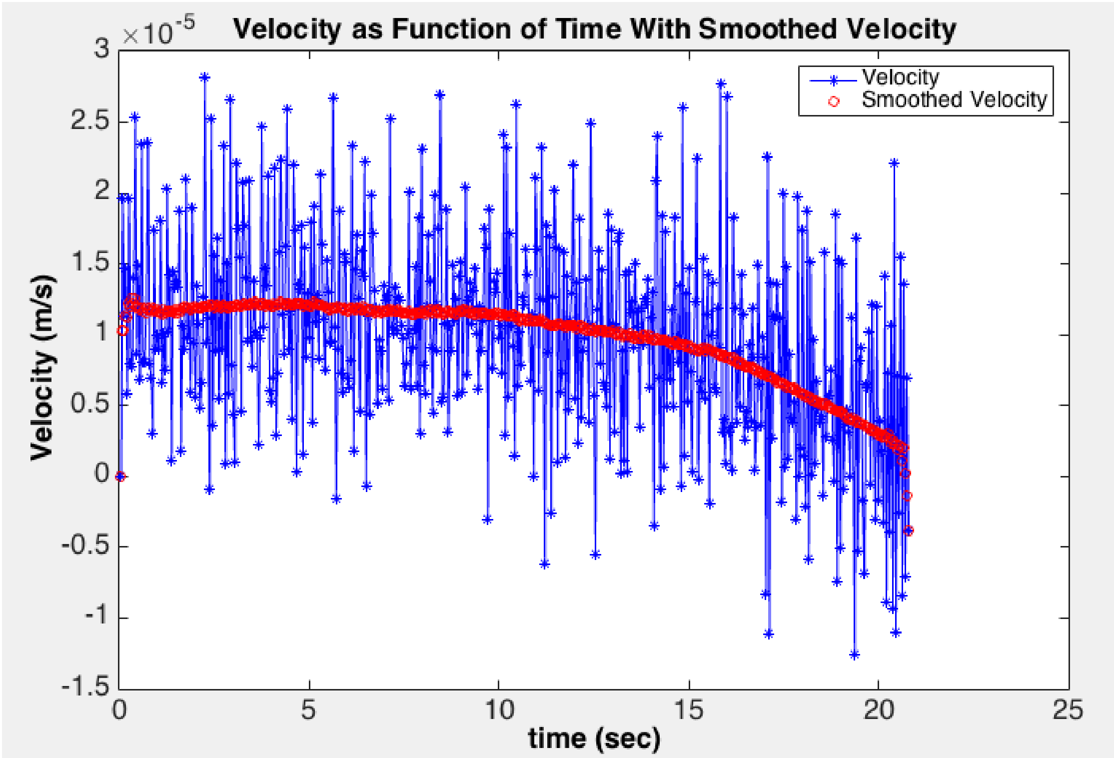

Figure 5.12: Velocity versus time for perpendicular moving island with reduced radius $a/l_s = 0.5847$. The blue line is the raw velocity calculated from the change in separation distance per time. The smoothed velocity averages over 100 data points.

The difference between the two different films these three islands are observed on is that the film with the two islands with reduced mobility $a/l_s = 0.5847$ and $a/l_s = 0.6608$ was tilted and 2 minutes later the data collection began. The film with the island with reduced radius $a/l_s = 4.4741$ was tilted and 10 minutes later the data collection began. The speculation worth exploring is that when the film is tilted the fluid comprising the meniscus flows from the top around the boundary until it settles at the bottom of the film. The film that was allowed 10 minutes to settle before data collection began may have had sufficient amount of time for the meniscus fluid to settle compared to the film that was only given 2 minutes. Furthermore, the two islands on the film given 2 minutes to settle hit the boundary and then both turned and flowed parallel along the boundary in the same direction. This may be indicative of flow in the film around the boundary. The island on the film given 10 minutes to settle hit the boundary and parked itself; it did not continue to flow

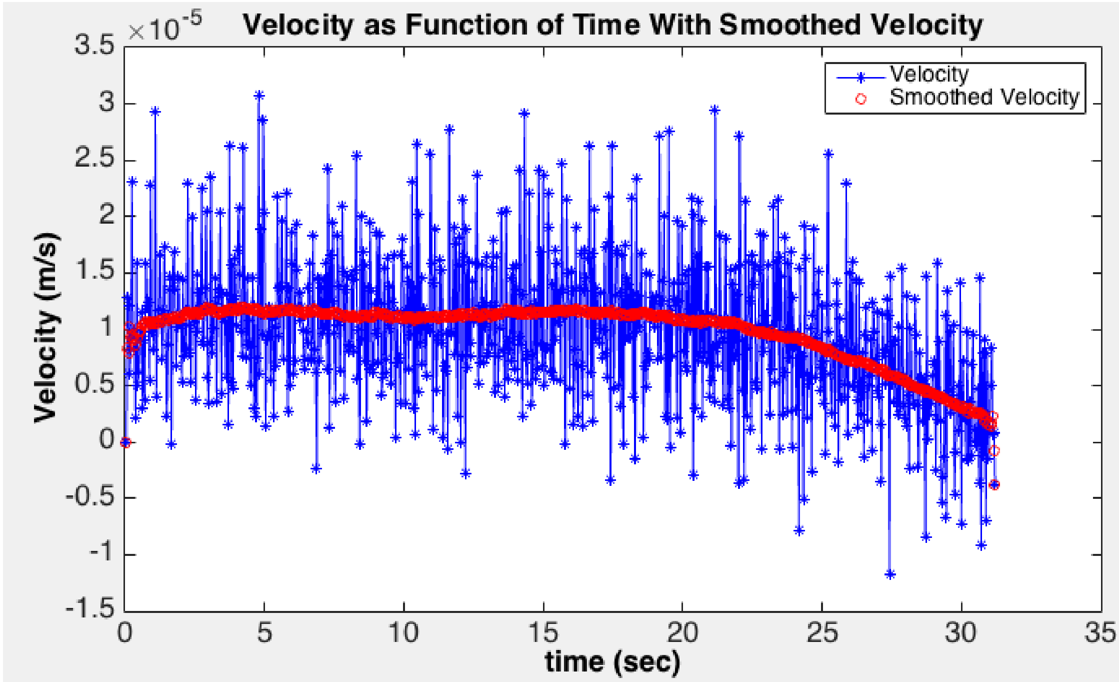

Figure 5.13: Velocity versus time for perpendicular moving island with reduced radius a/l_s = 0.6609. The blue line is the raw velocity calculated from the change in separation distance per time. The smoothed velocity averages over 100 data points.

parallel to the boundary.

Consider now the two islands on the same film with reduced radius $a/l_s = 0.5847$ and $a/l_s = 0.6608$ with thicknesses of 10 and 15 layers, respectively. The $a/l_s = 0.5847$ island has a greater reduced mobility than its sister island. Since reduced mobility scales as $\mu = v_d/F$ where $F = m\vec{g}$ and where the velocities of the two islands are very similar, then since the mass scales with the film thickness, it makes sense that the island $a/l_s = 0.5847$ with 75% of the mass of the sister island would have a greater reduced mobility.

5.3 Tilting Film Experiment: Parallel Case

Seven islands moving parallel to the boundary were studied where each island generated a single data point. All of the islands were on a film 6 layers thick and tilted at 2.6 degrees from the horizontal. The thicknesses of the islands were 9, 11, 12, and 13 layers. The diameters ranged from

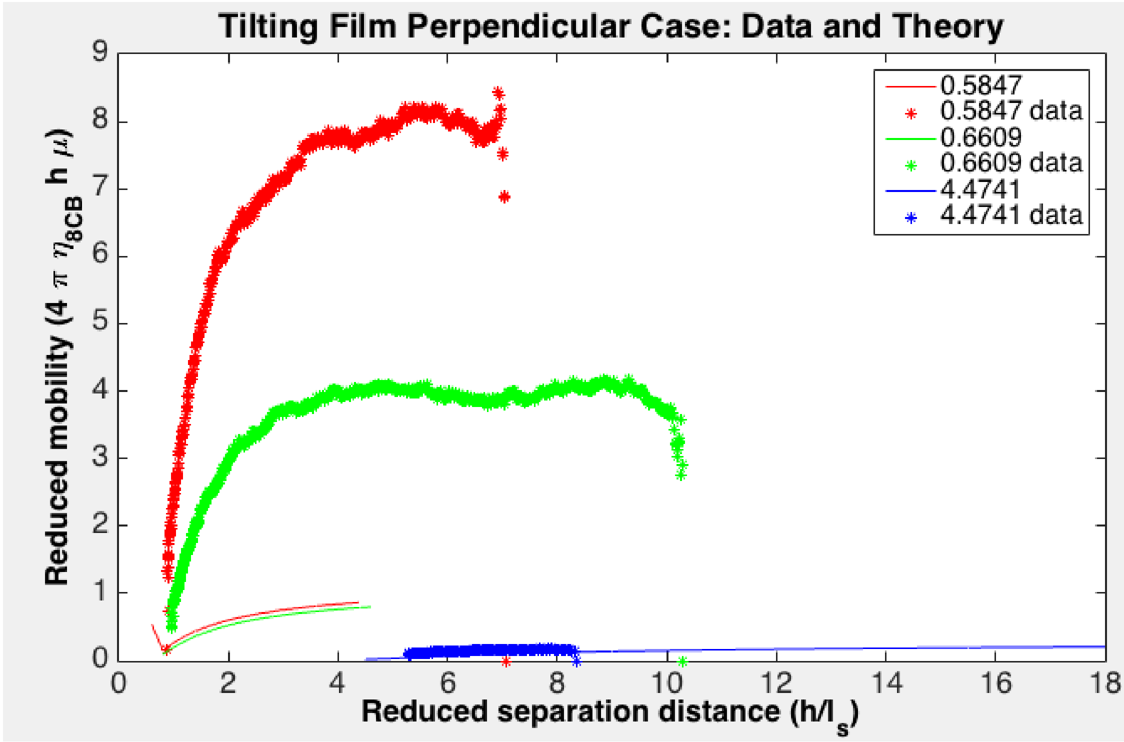

Figure 5.14: Reduced mobility for islands with reduced radius $a/l_s = 0.5847$, $a/l_s = 0.6609$, and $a/l_s = 4.4741$ compared to theory. Theory marked by solid lines while data marked by a star. The data for the island with reduced radius $a/l_s = 4.4741$ is better visible in Figure 5.11.

37 pixels to 110 pixels. Figure 5.15 is the velocity and smoothed velocity for the island with the smallest reduced mobility. Figure 5.16 is the velocity and smoothed velocity for the parallel island with the greatest reduced mobility.

Here it is observed that the island with the smallest reduced mobility has the reduced radius of $a/l_s = 0.9829$ and also was the first island tracked once the film was tilted. This island has an average velocity increasing from 0 m/s to $0.5 \times 10^{-5} m/s$. The island with the greatest reduced mobility has the reduced radius of $a/l_s = 0.627$ and has an average velocity of $2.5 \times 10^{-5} m/s$ which is more than 5 times faster than the $a/l_s = 0.9829$ island. Figure 5.17 shows the theoretical curves corresponding to all of the islands, however, only the $a/l_s = 0.9829$ island's data point is visible on this scale. The rest of the data points are seen in Figure 5.18, all of which are significantly greater than the theoretical curve.

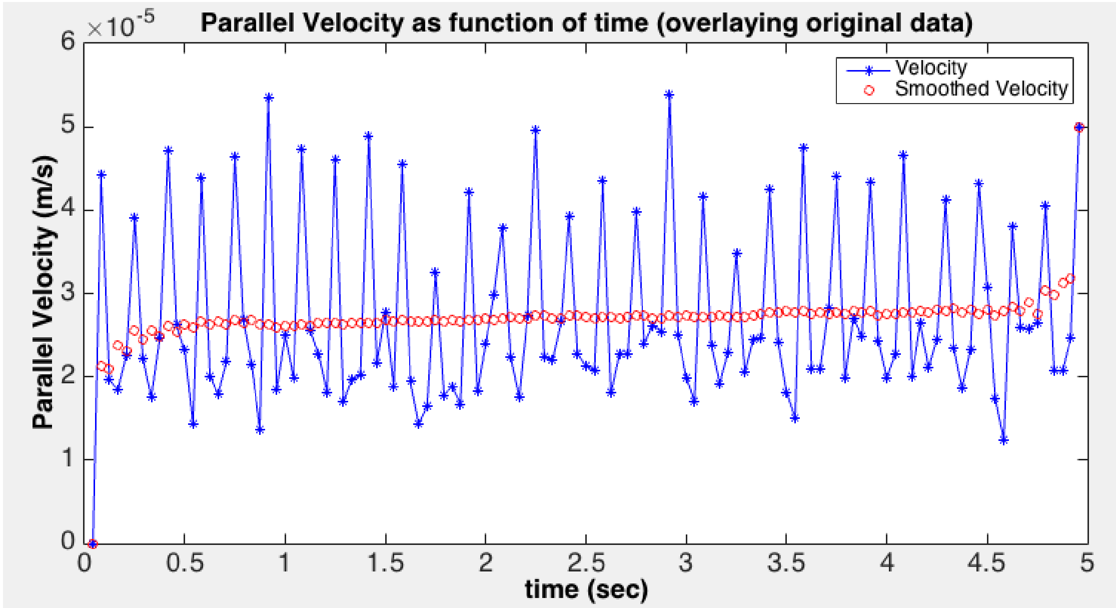

Figure 5.15: Velocity versus time for parallel moving island with reduced radius $a/l_s = 0.627$ tilted at 2.6 degrees. The blue line is the raw velocity calculated from the change in separation distance per time. The smoothed velocity averages over 100 data points.

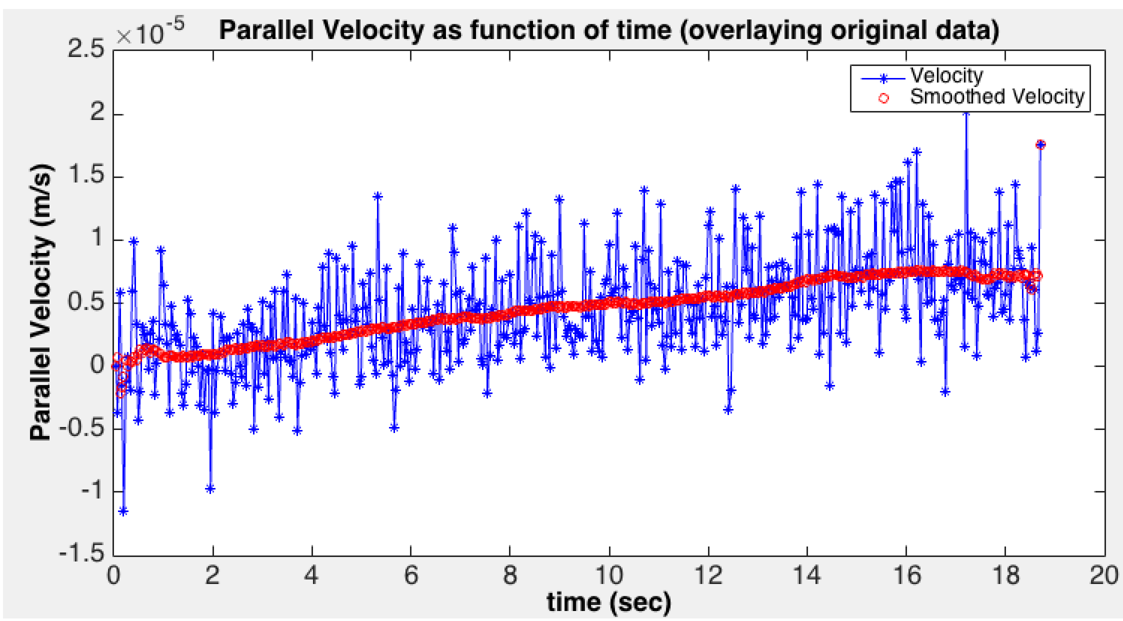

Figure 5.16: Velocity versus time for parallel moving island with reduced radius $a/l_s = 0.9829$ tilted at 2.6 degrees.. The blue line is the raw velocity calculated from the change in separation distance per time. The smoothed velocity averages over 100 data points.

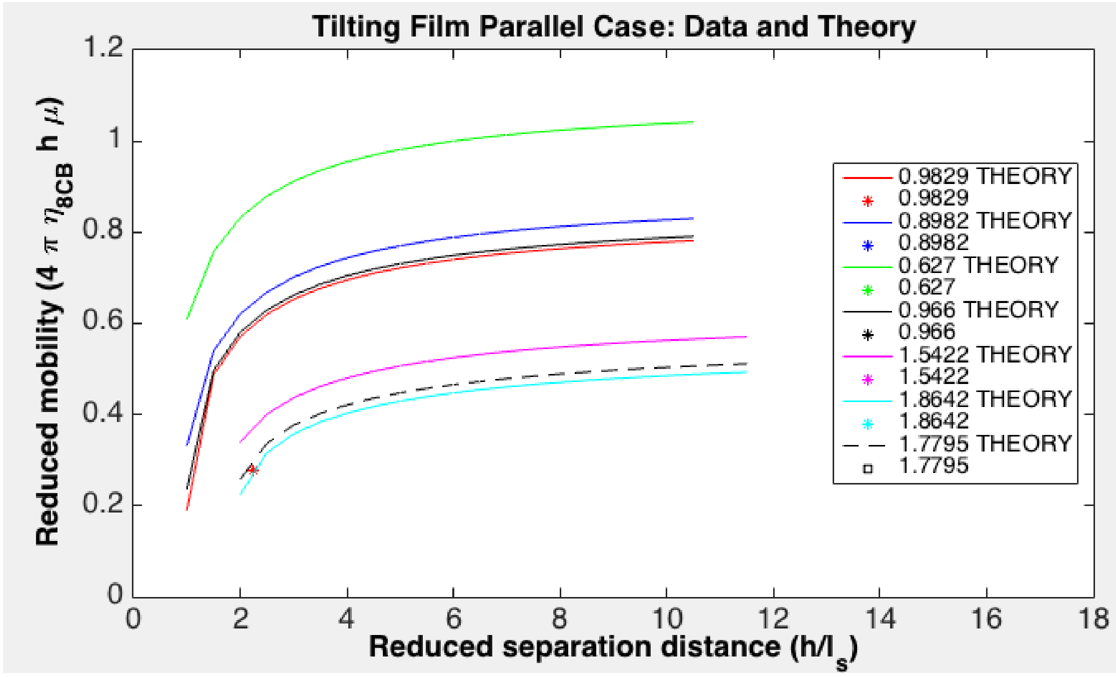

Figure 5.17: Reduced mobility as function of separation distance for all parallel moving islands compared to theory. Theory marked by solid lines line while data marked by a star. Only the data for the island with reduced radius $a/l_s = 0.9829$ is visible here. The rest of the data is visible in Figure 5.18.

Another interesting observation of the island with reduced radius $a/l_s = 0.627$ is that there appears to be fluid flow under the glass of the boundary. Recall that the film holder is glued to an aluminum piece that has a bigger hole cut into it. As a result there is a region between the hole the film is drawn across and the aluminum. The flow is observed in the videos of these islands by watching a particle trapped under the glass in the fluid, which is denoted as “Flowing Particle”. The particle travels at half of the velocity of the tracked island and in the opposite direction, which is up hill of the inclined film. Figure 5.20 illustrates the progression of the “Flowing Particle” compared to the tracked island.

Spurious fluids in motion indicates that there may be additional components to the dynamics of the film when tilted. For example, the spurious fluid motion observed as the movement of the flowing particle trapped under the glass film holder. It is possible that these additional fluid dynamics are not accounted for in the reduced mobility calculations and the increased reduced

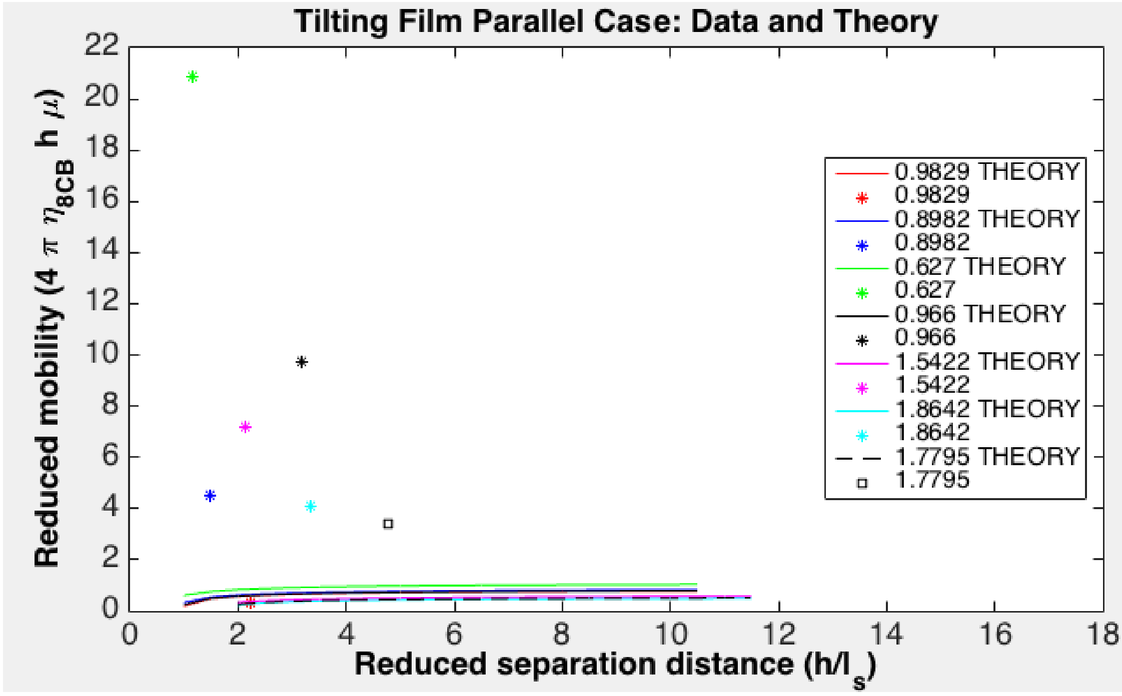

Figure 5.18: Reduced mobility as function of separation distance for all parallel moving islands compared to theory. Theory marked by solid lines while data marked by a star.

mobilities measured may be a result of this additional fluid movement. This observation may be indicative of a settling time protocol requirement for the film to be used in future trials.

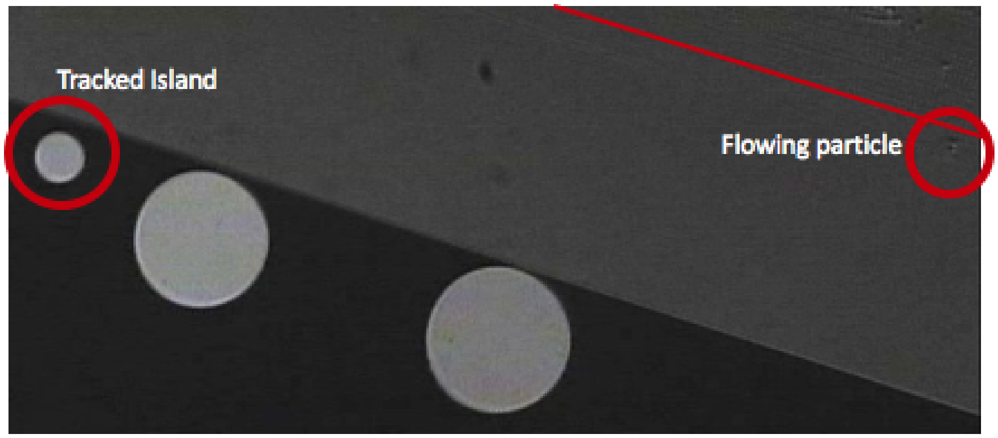
Tracked Island
Flowing particle

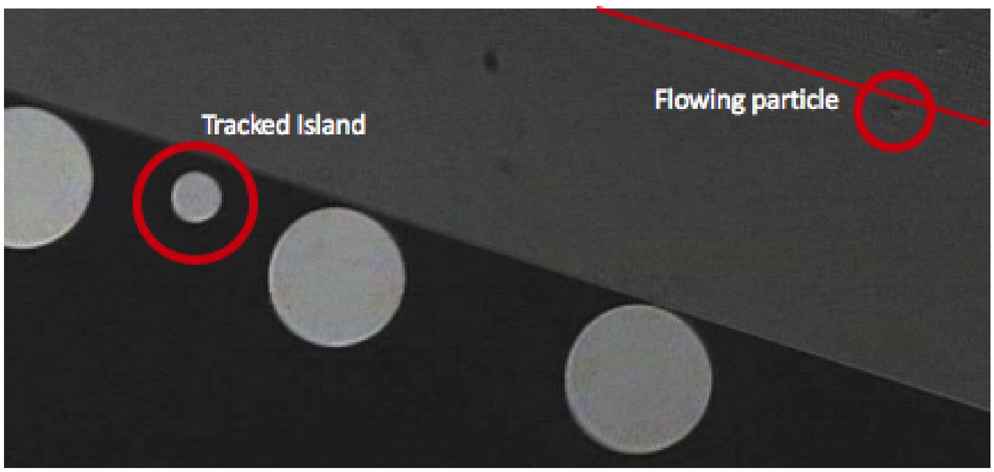
Flowing particle
Tracked Island

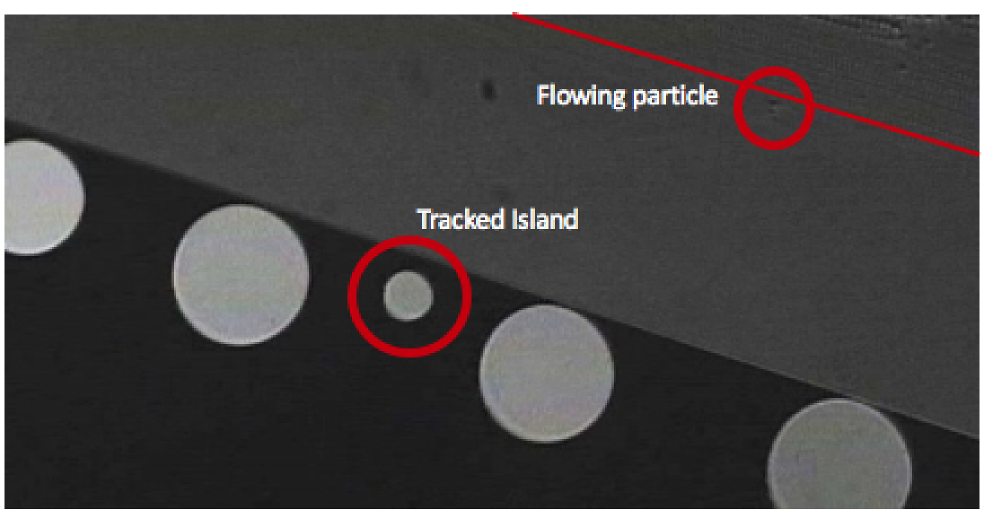
Flowing particle
Tracked Island

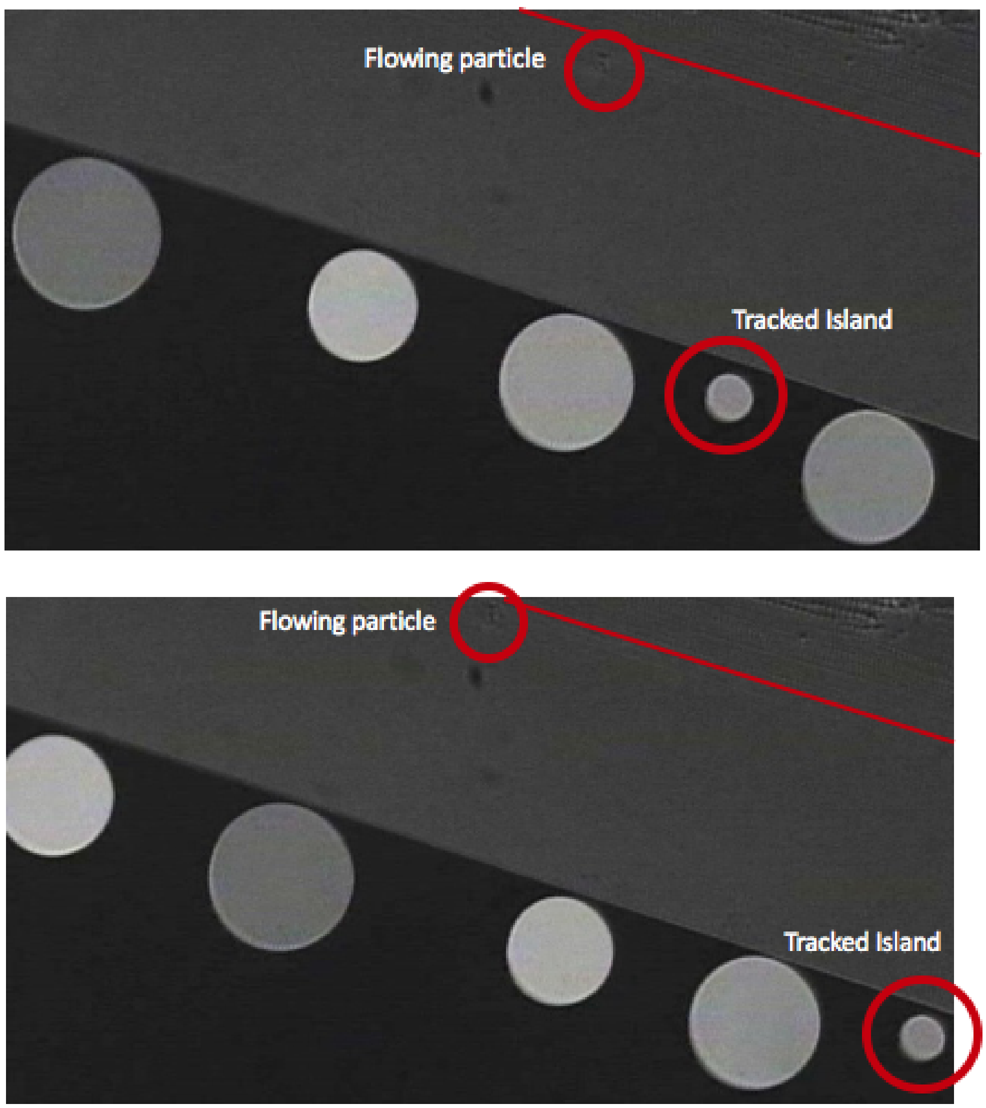

Figure 5.20: Still frame progression of tracked island and flowing particle. The tracked island is marked with the red circle and has reduced radius of $a/l_s = 0.627$ and has the greatest reduced mobility of the parallel moving island data. The flowing particle is also marked with a red circle and its path is traced with the red line.

Chapter 6

Conclusions

The crowding experiment resulted in many crowded particles with a reduced mobility greater than the isolated island HPW value. This is counterintuitive because it suggests that the islands are diffusing faster when surrounded by neighboring islands within a couple of Saffman lengths than when isolated. The IDL diffusion.pro program used for calculating the diffusion coefficients requires enhancement to better handle linear drift in the x and y directions. Whenever a particle has substantial drift in either direction the mean-squared displacement plot for the corresponding direction becomes "super-linear" where it curves up and away from the linear fitted polynomial. The minimum amount of linear drift diffusion.pro can handle in the x direction was found to be greater than in the y direction. Enhancements to diffusion.pro should include determining how to treat linear drift in these two directions equally.

Confinement effects were observed for islands and oil droplets that exhibit Brownian motion without substantial linear drift in that the mean-squared displacement plots roll over from the linear fitted polynomial in the first time lag. These confinement effects were not observed as a decrease in the reduced mobility. Furthermore, two islands of equal reduced radii exhibiting similar Brownian motion particle track without substantial drift and with roll overs in the mean-squared displacement plots for x and y resulted in one of the data points above the HPW curve and the other landing on the isolated island HPW value. The similar roll overs in the mean-squared displacements is indicative of similar crowding environments. Isolated islands on 7 layer films resulted in reduced mobilities above the HPW curve. The isolated island case provides the comparison platform for the crowding experiment.

Future work includes enhancing the diffusion calculations so the isolated island cases consistently hit the isolated island HPW values. Once this is achieved, then measurements of reduced mobility for crowded islands can be compared. Crowding quantification should not take place before the enhancements to calculating the reduced mobility are made.

Islands moving perpendicular to the boundary experiencing the force of gravity exhibited a decrease in reduced mobility as the islands approached the boundary. Additional fluid flow was observed in two of the three perpendicular moving islands once the islands hit the boundary they were both pulled in what appears to be a current running parallel to the boundary. This may be indicative that the film must be allowed sufficient time to settle before data is collected.

Islands moving parallel to the boundary experiencing the force of gravity exhibited reduced mobilities many times greater than the theoretical curve, with the exception of the first island observed in this run. Fluid flow under the glass beyond the boundary at half of the velocity of the islands moving next to the boundary was observed. It is possible that additional dynamics of spurious fluids not taken account for in the reduced mobility measurements may result in reduced mobilities that do not match the theoretical curves. All of the parallel islands were on the same film tilted at the same angle.

The image island method is still a valid method for understanding the dynamics of mutually interacting islands within a couple Saffman lengths. The results of both the perpendicular tilting film case and parallel tilting film case indicate additional components to the boundary fluid dynamics and that there may be unknown violations or properties that are not well understood in the assumed boundary conditions for a zero velocity flow field at the boundary when an island is drifting under the force of gravity. Spurious fluid movements of the meniscus and of islands near a boundary indicate that experimental enhancements or protocols are necessary. Both the parallel and perpendicular tilting film cases suggest the necessity for allowing the tilted film to settle before creating and observing islands.

Bibliography

[1] A. J. Leadbetter, J. L. A. Durrant, and M. Rugman, "The density of 4 n-octyl-4-cyano-biphenyl (8cb)," Molecular Crystals and Liquid Crystals, vol. 34, pp. 231–235, 1976.

[2] P. G. Saffman J. Fluid Mech., vol. 73, p. 593, 1976.

[3] P. G. Saffman and M. Delbrück, "Brownian motion in biological membranes," Proc. Natl. Acad. Sci. USA, vol. 72, p. 3111, 1975.

[4] M. J. Stephen and J. P. Straley, "Physics of liquid crystals," Rev. Mod. Phys., vol. 46, pp. 617–704, Oct 1974.

[5] J. H. N. D. S. W. J. L. M. V. J. T. Thomas Khn, Teemo Ihalainen, "Protein diffusion in mammalian cell cytoplasm," PLoS ONE, vol. 6, p. e22962, 2011.

[6] F. Z. R. J. M. S. H. S. T. S. F. S. Felix RoosenRungea, Marcus Hennig, "Protein self-diffusion in crowded solutions," PNAS, vol. 108, p. 1181511820, July 2011.

[7] M. D. E. G. P. S. W. Z. M. N. W. Sally Kim, Hugo Sanabria, "Quantifying translational mobility in neurons: Comparison between current optical techniques," J. Neurosci., vol. 30, p. 1640916416, Dec 2010.

[8] M. G. Friedel, The Mesomorphic States of Matter, vol. 1. Fort Belvoir, VA: U.S. Army Engineer Research and Development Laboratories., 1967.

[9] Laynetworks.com, "Molecular orientation in liquid crystal phases," (n.d.).

[10] D. Davidov, C. R. Safinya, M. Kaplan, S. S. Dana, R. Schaetzing, R. J. Birgeneau, and J. D. Litster, "High-resolution x-ray and light-scattering study of critical behavior associated with the nematic¯smectic-a transition in 4-cyano-4′-octylbiphenyl," Phys. Rev. B, vol. 19, pp. 1657–1663, Feb 1979.

[11] F. Schneider, "Measurement of the viscosity coefficient η_3 in free-standing smectic films," Phys. Rev. E, vol. 74, p. 021709, Aug 2006.

[12] P. Oswald and P. Pieranski, Smectic and Columnar Liquid Crystals: Concepts and Physical Properties Illustrated by Experiments, vol. 1. CRC Press, 2005.

[13] P. E. B. Weast and R. C., Handbook of Chemistry and Physics-54th Edition, vol. 1. CRC Press, Cleveland, 1973.

[14] D. F. Kelley, “Professor david f. kelley. website.,” (n.d.).

[15] P. P. et al., “Physics of smectic membranes,” Physica A, vol. 194, p. 364389, March 1993.

[16] L. D. M. J. Cavanagh, A., “Freely suspended films of smectic liquid crystal. website.,” (n.d.).

[17] J. E. M. A. Pattanaporkratana, C. S. Park and N. A. Clark., “Manipulation of disk-shaped islands on freely suspended smectic films and bubbles using optical tweezers,” Ferroelectrics, vol. 310, p. 131136, 2004.

[18] Z. Qi, Z. H. Nguyen, C. S. Park, M. A. Glaser, J. E. Maclennan, N. A. Clark, T. Kuriabova, and T. R. Powers, “Mutual diffusion of inclusions in freely suspended smectic liquid crystal films,” Phys. Rev. Lett., vol. 113, p. 128304, 2014.

[19] R. Brown, The Miscellaneous Botanical Works of Robert Brown, vol. 1. R. Hardwicke, London., 1866.

[20] J. Fourier, Theorie Analytique de la Chaleur, vol. 1. Firmin Didot, 1822.

[21] A. Fick, “Diffusion of particles in free-standing liquid films,” Phil. Mag., vol. 10, p. 3039, 1855.

[22] G. G. Stokes, “On the effect of the internal friction of fluids on the motion of pendulums,” Cambridge Philos. Trans., vol. 3, p. 8106, 1851.

[23] J. Happel and H. Brenner, Low Reynolds number hydrodynamics: with special applications to particulate media. Mechanics of Fluids and Transport Processes Series, Martinus Nijhoff, 1965.

[24] A. Einstein, Investigations on the theory of Brownian Movement. Dover Publications, Inc., 1955.

[25] B. D. Hughes, B. A. Pailthorpe, and L. R. White, “The translational and rotational drag on a cylinder moving in a membrane,” J. Fluid Mech., vol. 110, pp. 349–372, 8 1981.

[26] E. Petrov and P. Schwille Biophys. J., vol. 94, p. L41, 2008.

[27] Z. H. Nguyen, M. Atkinson, C. S. Park, J. Maclennan, M. Glaser, and N. Clark, “Crossover between 2d and 3d fluid dynamics in diffusion of islands in ultrathin freely suspended smectic films,” Phys. Rev. Lett., vol. 105, p. 268304, 2010.

[28] T. Kuriabova. et al. (manuscript in preparation).

[29] V. Prasad, S. A. Koehler, and E. R. Weeks, “Two-particle microrheology of quasi-2d viscous systems,” Phys. Rev. Lett., vol. 97, p. 176001, Oct 2006.

[30] T. P. T. J. C. A. Catipovic, M.A., “Improving the quantification of brownian motion,” Am. J. Phys., vol. 81, p. 485491, July 2013.

[31] R. A., “Brownian motion and single particle tracking,” Advanced Bioengineering methods laboratory, p. 123.

[32] R. A., “Simulating brownian motion,” Advanced Bioengineering methods laboratory, p. 114.

[33] C. Cheung, Y. H. Hwang, X.-l. Wu, and H. J. Choi, "Diffusion of particles in free-standing liquid films," Phys. Rev. Lett., vol. 76, pp. 2531–2534, Apr 1996.

[34] P. Cicuta, S. L. Keller, and S. L. Veatch, "Diffusion of liquid domains in lipid bilayer membranes," J. Phys. Chem. B Lett., vol. 111, pp. 3328–3331, March 2007.

[35] J. C. Crocker, M. T. Valentine, E. R. Weeks, T. Gisler, P. D. Kaplan, A. G. Yodh, and D. A. Weitz, "Two-point microrheology of inhomogeneous soft materials," Phys. Rev. Lett., vol. 85, pp. 888–891, Jul 2000.

[36] A. Eremin, S. Baumgarten, K. Harth, R. Stannarius, Z. H. Nguyen, A. Goldfain, C. S. Park, J. E. Maclennan, M. A. Glaser, and N. A. Clark, "Two-dimensional microrheology of freely suspended liquid crystal films," Phys. Rev. Lett., vol. 107, p. 268301, Dec 2011.

[37] A. J. Levine and F. C. MacKintosh, "Dynamics of viscoelastic membranes," Phys. Rev. E, vol. 66, p. 061606, Dec 2002.

[38] A. J. Levine, T. B. Liverpool, and F. C. MacKintosh, "Mobility of extended bodies in viscous films and membranes," Phys. Rev. E, vol. 69, p. 021503, Feb 2004.

[39] E. P. Petrov, R. Petrosyan, and P. Schwille, "Translational and rotational diffusion of micrometer-sized solid domains in lipid membranes," Soft Matter, vol. 8, no. 29, pp. 7552–7555, 2012.

[40] Z. Qi, C. S. Park, M. A. Glaser, J. E. Maclennan, and N. A. Clark, "Experimental realization of an incompressible newtonian fluid in two dimensions," submitted to Phys. Rev. E, 2016.

[41] Z. Qi, Ph. D. thesis. University of Colorado, 2015.

```
function [] = KP_b3_11 ( m, n, d, t, xDrift, yDrift, nlags );
close all;
clc;
% Kaitlyn Parsons
% Brownian Motion simulation
% inputs: dimension (m), number of frames (n), diffusion coefficient (d), total amount↙
of time (t), linear drift in x direction (xDrift) and y direction (yDrift)
%       number of time lags for MSD calculation (nlags)   % jem
% References in Thesis.
% Radenovic A., “Brownian motion and single particle tracking,” Advanced↙
Bioengineering methods
%laboratory, p. 123.





outputDirectory = '/Users/KaitlynParsons/Desktop/March13';
%create output directory
if ~exist(outputDirectory,'dir')
     mkdir(outputDirectory);
end
%%%%%%%%%%%%%%%%%%%%%%%%%%      PROMPTS           %%%%%%%%%%%%%%%%%%%%%
prompt1 = 'Enter the number of dimensions (default is 2) m = ';
m = input(prompt1);
if isempty(m) == 1
    m = 2;
    fprintf ( 1, '\n' );
    fprintf ( 1, '  Using default spatial dimension m = %g\n', m );
    fprintf ( 1, '\n' );
    clc;
end

prompt2 = 'Enter the number of frames (default is 10000) n = ';
n = input(prompt2);
if isempty(n) == 1
    n = 10000;
    fprintf ( 1, '\n' );
    fprintf ( 1, '  Using default number of frames n = %g\n', n );
    fprintf ( 1, '\n' );
    clc;
end

prompt3 = 'Enter the diffusion coefficient (default is 0.25 microns^2/s) D = ';
D = input(prompt3);
if isempty(D) == 1
    D = 0.25;
    fprintf ( 1, '\n' );
    fprintf ( 1, '  Using default diffusion coefficient D = %g\n', D );
    fprintf ( 1, '\n' );
    clc;
end

prompt4 = 'Enter the frames rate (default is 50) fps = ';
fps = input(prompt4);
if isempty(fps) == 1
    fps = 50;
    fprintf ( 1, '\n' );
    fprintf ( 1, '  Using default frame rate fps = %g\n', fps );
    fprintf ( 1, '\n' );
    clc;
```

```
end

prompt5 = 'Enter the x drift constant (default is 0) xDrift = ';
xDrift = input(prompt5);
if isempty(xDrift) == 1
    xDrift = 0.0;
    fprintf ( 1, '\n' );
    fprintf ( 1, '  Using default xDrift = %g\n', xDrift );
    fprintf ( 1, '\n' );
    clc;
end

prompt6 = 'Enter the y drift constant (default is 0) yDrift = ';
yDrift = input(prompt6);
if isempty(yDrift) == 1
    yDrift = 0.0;
    fprintf ( 1, '\n' );
    fprintf ( 1, '  Using default yDrift = %g\n', yDrift );
    fprintf ( 1, '\n' );
    clc;
end

prompt7 = 'Enter the number of time lags = ';
nlags = input(prompt7);
if isempty(nlags) == 1
    nlags = 100;
    fprintf ( 1, '\n' );
    fprintf ( 1, '  Using default nlags = %g\n', nlags );
    fprintf ( 1, '\n' );
    clc;
end
%%%%%%%%%%%%%%%%%%%%%%%%%%      CALCULATIONS        %%%%%%%%%%%%%%%%%%%%%
dt = 1/fps ;  % time per frame

%tau = nlags*dt;
tau = dt;

alpha = sqrt(2*D*dt);
% -------------------------------------------------------
% dx = alpha*randn(n,1) + xDrift*alpha;
% dy = alpha*randn(n,1) + yDrift*alpha;
sigma = sqrt(2*D*dt);      % jem
mu=0.0;
dx = normrnd(mu,sigma,n,1) + xDrift*alpha;
dy = normrnd(mu,sigma,n,1) + yDrift*alpha;

% make sure the distribution is what we are trying for jem
% Calculate the sample mean, standard deviation, and variance
stats = [mean(dx) std(dx) var(dx)];
disp(['sigma ' num2str(sigma) ]);
disp([' fps   ' num2str(fps) ]);
disp(['dt '  num2str(dt) ]);
disp(['mean std var ' num2str(stats) ]);




% -------------------------------------------------------



x = cumsum(dx);
y = cumsum(dy);
```

```
dmsd = dx.^2 + dy.^2;
MSD = cumsum(dmsd);
MSDx = cumsum(dx.^2);
MSDy = cumsum(dy.^2);
% msd = x.^2 + y.^2;
%
% msd_plot_data = zeros(n,1);
% for i = 1:n
%     msd_plot_data(i) = sum(msd(i:n)) / (n-i);
% end
%%%%%%%%%%%%%%%%%%%%%%%%%%      PLOTTING        %%%%%%%%%%%%%%%%%%%%%
H = figure('position',[150,100,1400,500],'Name','Brownian Motion Simulation by↙
Kaitlyn','color',[1,1,1]);

    hold on

% ------------------------------------------------------
    nbins1 = 50;        % jem just set the number of bins in the histograms
    % subplot(3,2,1), histfit(dx,round(n/bin));
    subplot(3,2,1), histfit(dx,nbins1);

    xlabel('displacement (microns) ');
    ylabel('frequency (displacement)');
    title('X displacement histogram');
    [muX,sigmaX] = normfit(dx);     % note you already get this from histfit jem
    % disp([ 'Dx = ' num2str(sigmaX^2 /2 /dt/bin) ]);
    disp([ 'Dx = ' num2str(sigmaX^2 /(2 * dt)) ]);  % jem
    hold off

    hold on
    % subplot(3,2,3), histfit(dy,round(n/bin));
    subplot(3,2,3), histfit(dy,nbins1);
    Facecolor = 'blue';
    xlabel('displacement (microns) ' );
    ylabel('frequency (displacement)');
    title('Y displacement histogram');
    [muY,sigmaY] = normfit(dy);
    % disp([ 'Dy = ' num2str(sigmaY^2 /2 /dt/bin) ]);
    disp([ 'Dy = ' num2str(sigmaY^2 /(2 * dt)) ]);  % jem
    hold off
% ------------------------------------------------------

    hold on
    time = 1:nlags;   % units of frames
    %time = time*dt; % untis of sec
    time = time';
    P = polyfit(time,MSD(time),1);
    curve = P(1)*time + 0;
    disp(['msd Slope ' num2str(P(1)/4/tau) ]);
    subplot(3,2,5), plot(time,MSD(time),time,curve(time));
    ylabel('Mean-squared displacement (micron^2)');
    title('Mean-squared displacement with fitted line through orign');

    hold off
   %plot(time, (0:1:(N-1)) * 2*k^2 , 'b', 'LineWidth', 3)

for i=1:nlags:n,

    if ~ ishandle(H) || strcmp(get(H, 'currentCharacter'),'b'),
        close all;
        break;
```

```
    end

    subplot(1,2,2), plot(x(1:i),y(1:i),'Color','b');
%     'Color',[.4,1,.2]);
    title('Simulated Brownian Motion Track');
    xlabel([ 'microns After ' num2str(round(i*dt)) 's of total ' num2str(round(n*dt))↙
's.' ]);
    ylabel('microns')
    pause(0.02);
end

C = zeros(n,1);
    for i = 1:n
        C(i)=i;
    end

    F = [ C, x, y, C, C, C];     % Output x and y coordinates
    if xDrift == 0 && yDrift == 0;              % NO DRIFT!
       save BM_NODrift.epx F -ASCII
    else
        save BM_Drift.epx F -ASCII
    end

end
```